QATAR UNIVERSITY

COLLEGE OF ENGINEERING

COUPLED CFD-DEM PARALLEL MODEL TO DESCRIBE FINE MIGRATION BEHAVIOR AT THE PORE-SCALE

BY

AHMED SAMI ELRAHMANI

A Thesis Submitted to

the College of Engineering

in Partial Fulfillment of the Requirements for the Degree of

Master of Science in Environmental Engineering

January 2021

COMMITTEE PAGE

The members of the Committee approve the Thesis of
Ahmed Sami Elrahmani defended on 06/12/2020.

Prof. Riyadh Al-Raoush
Thesis/Dissertation Supervisor

Dr. Thomas Daniel Seers
Committee Member

Dr. Ibrahim Mohamed Husien Abu-Reesh
Committee Member

Approved:

Khalid Kamal Naji, Dean, College of Engineering

ABSTRACT

ELRAHMANI, AHMED, S., Masters : January : 2021, Masters of Science in Environmental Engineering

Title: Coupled CFD-DEM Parallel Model to Describe Fines Migration Behavior at the Pore-Scale

Supervisor of Thesis: Prof. Riyadh, I, Al-Raoush.

Transport of fine particles in porous media has attracted considerable interest over the past few decades. In various fields of science and engineering, on-site remediation strategies, enhanced transport of contaminants into aquifers, artificial recharging of groundwater aquifers, and permeability of oil and gas reservoirs have become topics of concern. Much research projects focused on the development of models that can predict their behavior on a pore-scale level. The model described here uses a Computational Fluid Dynamics – Discrete Element Method (CFD-DEM) parallel model to simulate fine particle migration and interactions in porous media. The model was parallelized using Message Passing Interface (MPI) for communication between processors to achieve faster computation.

Model validation was performed by confirming the fluid flow separately using two geometries. Then, the coupled CFD-DEM model was validated by comparing its results to a micromodel experiment with the equivalent geometry. Comparison was done by utilizing different computer vision techniques to capture the behavior of the particles throughout the micro-model experiment. The CFD-DEM was able to capture the particles transport in porous media while maintaining low computational cost with the use of parallelization. The open-source library OpenCV showed great potential to

be used for image and video processing for the results captured from micromodel experiments, which could be used for coupled model validations as well as data analysis in future research.

DEDICATION

To who believed in me, words are certainly not enough to thank you.

To my parents.

ACKNOWLEDGMENTS

I would like to express my sincere gratitude to God Almighty for all the blessings and mercy for the successful completion of this thesis.

Many thanks to my supervisor, Prof. Riyadh Al-Raoush, for his incredible support, guidance, valuable advice, and constructive criticism that led to the successful completion of this work. I am grateful for all my research colleagues in Prof. Riyadh's group at Qatar University. Many thanks to Eng. Hamza Abugazia for his help and support in many ways in my thesis work. I am indebted to the entire department of Environmental Engineering at Qatar University for their excellent collaboration and support.

I would like to express my deepest gratitude to my family: my father, mother, brother, and sisters for their immense support and encouragement to achieve this degree.

TABLE OF CONTENTS

LIST OF TABLES

LIST OF FIGURES

CHAPTER 1: INTRODUCTION

1.1. Overview of fine migration in porous media

Fine particles are small particles with a diameter of fewer than 75 μm, that present in porous media (Frimmel, Kammer, and Flemming 2007). Fine particles have relatively wide surfaces and large electrical unbalanced charges on their surfaces in addition to their small size (Frimmel et al. 2007). The effect of the electrical forces on fines is thus greater than the gravimetric ones, which enables fines to suspend and float with the fluid flow through pores. Fine particles are divided into organic, inorganic, and biological particles. When the pore system consists of a continuous phase (the pore fluid) and dispersed phase (the fine particles), it is commonly known as a colloid, where the colloidal/fine particles, have an average size between 1 nm and 1 μm. Over the past few decades, the transport and fate of fines in porous media have gained more attention by several researchers due to its importance in several industrial and environmental applications (Cao et al. 2018; Chequer and Bedrikovetsky 2019; Han et al. 2019; Jang et al. 2018; Jarrar et al. 2018). Besides, the migration of fines can affect other fields such as geotechnical, hydraulic, environmental, and petroleum engineering (Kartic and H. Scott 1998). Fines migration in oil reservoirs, known as sandstone water sensitivity, is one of the most common practical effects of fines migration in petroleum engineering (Khilar and Fogler 1983). This migration can lead to a significant permeability reduction resulting in a significant reduction in oil production. The water sensitivity occurs when the sandstone formation is contacted by relatively freshwater (Shedid and Saad 2017; Zhang et al. 2019; Zhao et al. 2020).

Fine particle migration can also contribute to soil erosion in and on the surface in both natural and compacted soil. Hydrodynamic forces resulted from the drainage of the water could release fine particles, mainly in clay, so that these fines move by the

drainage flow which causes erosion in the soil. This type of soil erosion can cause serious problems in the geotechnical engineering applications, including dams and road failures (Nguyen et al. 2017; Richards and Reddy 2007; Vaidya and Fogler 1990). Moreover, it has been shown that the movement of colloid particles, like clay particles, help in diffusing the contamination and pollute groundwater. Mobile colloidal fines may adsorb and stabilize organic and inorganic contaminants in groundwater and therefore increase the number of pollutants transported by the groundwater (Corapcioglu and Jiang 1993; Frimmel et al. 2007; de Jonge, Kjaergaard, and Moldrup 2010).

Porous media are commonly used in other environmental applications, including the filtration of water and wastewater. Consideration for the colloidal particle transport is given to prevent trappings or clogging in the filter's bed when designing these operations (Datta and Redner 1998; Rodgers, Mulqueen, and Healy 2010; Sherard, Dunnigan, and Talbot 2002).

Further to this, the migration of fine particles during methane extraction by depressurization from gas-hydrate sediments could cause pore-throat clogging, depending on the topology and the geometry of the porous media. Thus, in order to predict the performance of gas hydrate reservoirs, it is essential to understand the fine migration role in gas hydrate sediments (Jung et al. 2012; Uchida et al. 2017; Waite et al. 2018). As a result of its wide applications, research into fines migration in porous media has increased to reach a total of 433 research papers published in this area from the year 2000 to 2019 , across multiple disciplines (Figure.1).

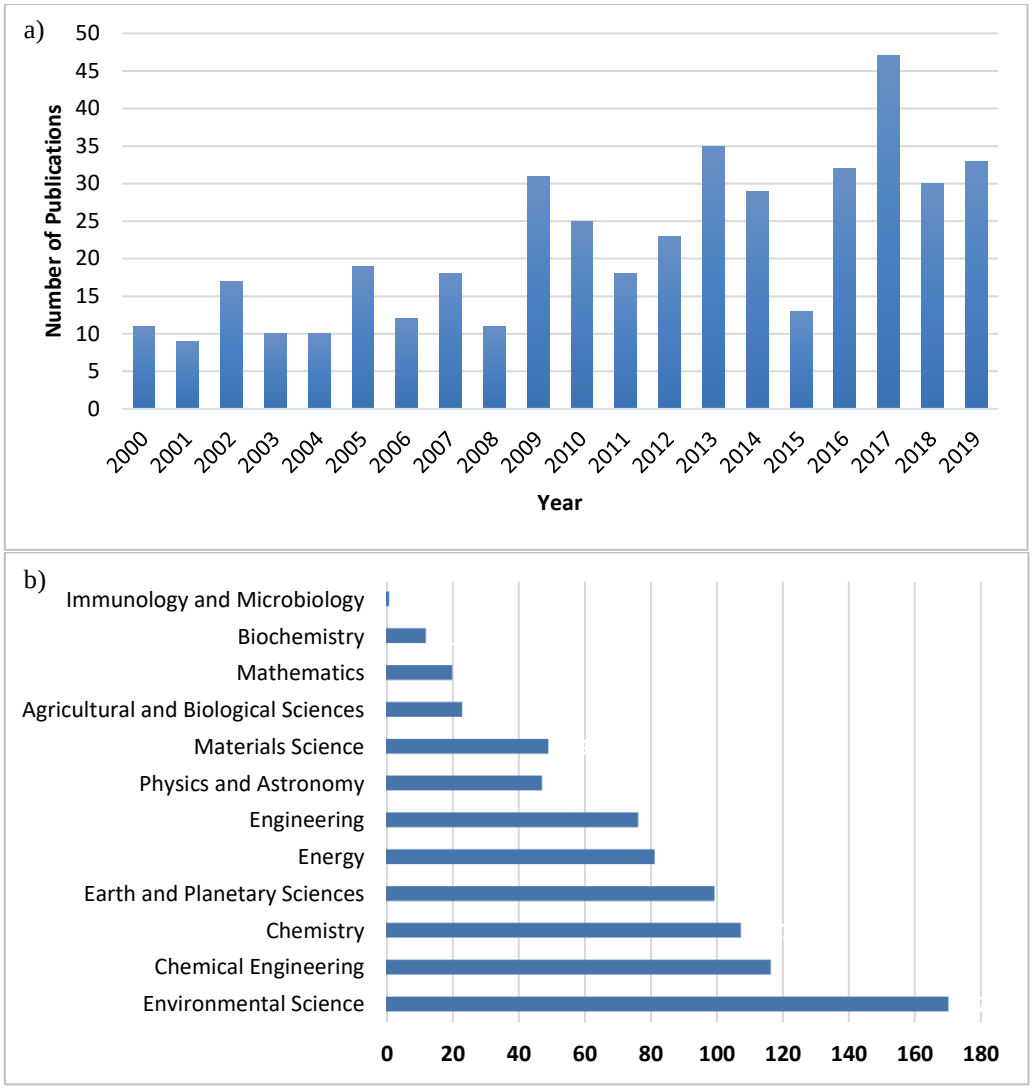

Figure 1 Fines migration publications statistics: (a) Number of publications per year and (b) number of publications per subject area (Source from Scopus Database, 2019)

1.2. Overview of modeling of fine migration in porous media

As a result of its wide applications, researchers have focused on developing models that can describe and predict the migration of fine particlesin porous media at a pore-scale level. Hirabayashi et al. used a two-phase Lattice Boltzmann Method (LBM) to investigate the fine particle size distribution effect on the permeability reduction in porous media (Hirabayashi et al. 2012). However, the grain particle representation in their model was unrealistic and ignored irregularities in geometry; hence, many

parameters were not accounted for in the model. Boccardo et al. used micro-scale Computational Fluid Dynamics (CFD) along with colloid filtration theory to simulate fine particle deposition in different porous media size and geometry (Boccardo, Marchisio, and Sethi 2014). Nevertheless, the model used a two-dimensional representation of the geometry and ignored the particle-particle interactions. Li & Prigiobbe (2018) as well as Zhou et al. (2018) used coupled LBM with Discrete Element Method (DEM) coupled using Immersed Boundary Method (IBM) to understand the raw behavior of migrating fine particles with different sizes and how it may affect the fluid flow in porous media (Li and Prigiobbe 2018; Zhou et al. 2018). Additionally, Su et al. (2019), developed an Efficient spheRical partIcle and Geometry Interaction Detection (RIGID) algorithm for a coupled CFD-DEM model to study the particles clogging mechanisms and their impact on the porous media flow (Su et al. 2019). The three latterly presented models had a limited number of simulated particles, possibly due to computational cost. Furthermore, the geometric representation was only two dimensional, which does not capture the full behavior of the clogging and assumes cylindrical fine particles along with an extruded depth (Li and Prigiobbe 2018; Su et al. 2019; Zhou et al. 2018). Moreover, the validation methods for all of the previously mentioned literature were very restricted, where none of them were compared to experimental results that capture the full physical behavior. Su et al. performed a limited validation of the presented model by subdividing the model into much simpler problems and validating each one separately (Su et al. 2019).

1.3. Thesis organization

The organization of this thesis is as follows: a comprehensive literature review to capture the studies that considered the mechanical and chemical processes affecting the fine migration in porous media, then the model structure as well as the

parallelization scheme was optimized for acquiring the best performance. The model presented uses a parallel CFD-DEM coupled model using Fully resolved Immersed Boundary Method (IBM) to predict the behavior of fine particle mobilization and interactions in pore-scale level porous media. The model geometry was captured from realistic porous media and represented as three-dimensional geometry. The model was validated by comparing its results to a micromodel experiment for the same geometry. The comparison was accomplished by imaging the lab results and evaluating particle motion using various computer vision techniques.

1.4. Objectives

- Use micro-scale sediment sample images to generate realistic geometry for the fine migration model.
- A couple between CFD- DEM using IBM to generate a model that can capture fines migration behavior in porous media.
- Achieve faster computation time by optimizing the number of processors in parallelization of the model.
- Use computer vision techniques for video processing of the captured results from the micromodel experiment.
- Validate the model compared to the experimental results to ensures the model's ability to capture the physical behavior.

CHAPTER 2: LITERATURE REVIEW

Generally, the migration of fines has three main effects on the pore system. It can (1) reduce the chemical reactivity of the system, (2) facilitate the contaminant's transport, and (3) cause physical changes to the pore structure (Frimmel et al. 2007). In the subsurface contaminants are often adsorbed to the solid phase surface or dissolved at the aquatic phase. The solid phase is generally considered fixed; however, fines can operate as a mobile contaminant carrier because of their release and resuspension in the system. Additionally, since fines have a considerably large specific surface area, a significant portion of the total surface area of the system will be eliminated which will cause a drop in the sorption capacity of the porous media as a system. Furthermore, the hydraulic characteristics of porous media in the subsurface may be modified as a result of particle deposition as well as release, as extensive as structural damages, the possible consequences include the complete clogging of the porous media. Two mechanisms are involved in the migration of fines in a single-phase flow (Cao et al. 2018). Firstly, particles block pore throats due to the size or concentration of particles. The second aspect is the chemical processes where partial particles, which are too small to clog pores, can cluster and become more effective to block certain pore throat diameters. Previous researches reviewed the fine migration in porous media from different aspects: (Kanti Sen and Khilar 2006) presented a review of fine particles facilitated transport of contaminants as well as their role in clogging pore throats. The authors included several parameters that affect the behavior of clogging in single-phase flow. (Molnar et al. 2015) had the aim of clarifying the roles of different pore and continuum scale modeling approaches in determining the discussed colloid transport in single-phase flow. (Li, Liu, and Jiang 2017) provided a summary of the main factors affecting the migration and deposition of the fine particles

in fully saturated media. (Dressaire and Sauret 2017) reviewed the clogging mechanisms caused by the transport of colloidal particles in microfluidic channels. (Boccardo et al. 2020) provided a review of different numerical methods used to predict the transport of fine particles in porous media at the pore-scale, along with the methods for the upscaling the models from the pore scale.

2.1. Mechanical processes of fines in porous media

2.1.1. Theoretical studies on the mechanical processes

In general, three distinct mechanisms have been defined for fines migration in porous media, known as piping, when there is no interaction between fines and grain particles, bridging, which is the process of pore-filling or the initiation of the clogging, and complete clogging or aggregation (Kartic and Scott 1998). These mechanisms are classified based on two critical metrics; the ratio of pore width to the diameter of fine particle (o/d) and the diameter of the grain particle to the diameter of fines (D/d). Besides the geometric parameters of the system, fines concentration and flow rate are also considered important parameters to determine the behavior of fines in porous media (Agbangla, Climent, and Bacchin 2012; Muecke 1979; Zhou et al. 2018). The critical fines concentration is defined as the ratio of the injected fines to the pore fluid that encourages clogging to the system. Where clogging is more likely to occurs, as the concentration of the fine fraction increases in the system. The research alluded to above showed that when D/d ratio decreases from 40 to 12.5, critical fines concentration, as a volume ratio, increases from 0.35 % to 9 % (Bradford et al. 2009; Pandya, Bhuniya, and Khilar 1998). Also, when the concentration of fine particles is increased, it led to rapid clogging within the range of ($1.67 < o/d < 100$). However, for a high (o/d) ratio of more than 100, clogging may not be affected by the fine's concentration (Gruesbeck and Collins 2007; Muecke 1979; Pandya et al. 1998). The flow rate required for

clogging increases by decreasing the concentration of the fine particles. At higher flow rates the fine particles are prevented from accumulating around the pore throats, known as bridging, due to disturbances in pressure and the high shear force caused by the flow. While at lower flow rates more particles are retained in the system (Agbangla et al. 2012; Muecke 1979).

2.1.2. Micro-scale experiments on the mechanical processes

Several studies have aimed to understand the migration and interactions of fine particles at the micro-scale level since understanding the behavior at that level helps to understand the behavior on the scaled-up levels. The impact of fine particles size and the pore structure geometry on colloid dispersion with water-saturated micromodels was examined at the pore scale by Auset and Keller (2004). The authors examined the exclusion of colloids in porous media of various sizes using certain pore geometries to differentiate the process based on their comparative significance. Three micromodels with different patterns were developed, where the colloids used were made of latex polystyrene carboxylate-modified microspheres with four different diameters. The colloid concentration used was 10^6-10^7 colloids/ml. The study was conducted for four total pressure differences of 100, 500, 1000, and 1500 Pa and under different water saturation conditions. Results demonstrated that the bigger particles preferred to have more straight routes under these conditions, while particles with smaller size made more diversions. The dispersal scale at a specified flow rate was governed by the pore throats and the colloidal particle size in addition to the geometry of pore space. The dispersion coefficients, which represent the mixing caused by the spatial variations of the local (time-averaged) velocity (Chin 2006), have reduced as colloid sizes increase. These results stress the significance of anticipating colloidal dispersion of the relative size of the particle with regards to pore throats.

Subsequently, Wyss et al. (2006) researched the clogging of individual microchannels using microfluidic devices to examine the impact of flow rate, volume fraction, and pore-to-particle size ratio on clogging. The colloidal particles suspension was flowed through a single wide channel, followed by a collection of parallel tight tubes. The suspension flow rate was regulated through the tubes by setting the fluid pressure to a constant value over the tubes. The findings showed that clogging was poorly dependent on particles flow rate and volume fraction, rather, the number of particles pipe through the porous media without causing clogging was directly related to the pore-to-particle size ratio. The smaller ratio indicates fewer particles could pipe through porous media without causing clogging.

Isa et al. (2009) found that, in a pressure-driven flow of dense particle suspensions, if the flow rate was higher than a certain limit that contributes to causing clogging. The pressure-driven flow of concentrated colloids deposited in single-particle glass microchannels was explored using fast confocal microscopy with a real-time imaging used to explore the confinement of hard spheres suspension that flows into a rectangular channel. Results showed that a pressure-driven flow of dense particle suspensions caused clogging if a small number of particles created a bridge across the channel length or if the flow rate is higher than a certain limit. The results confirmed the existence of a critical flow velocity in which clogging takes place above. Moreover, it indicates that bridging of smaller particles may enhance the possibility of clogging.

Mustin and Stoeber (2010) explored the impact of the polydisperse suspension on channel blocking using lab experiments. In this context, particles in suspension have initially been defined based on their size distribution and then measured using microfluidic equipment for their deposition behavior. Four distinct polystyrene

particle suspensions were used with a two distinct volume fraction of 4% and 8% and average diameters of 0.47, 0.50, 1.4, and 1.5 μm. All microfluidic tubes had the same height of 30 μm and a variety of broad channels allowed the suspension to be transported to the entrances of different narrow tubes. The observations showed a proportional relationship between the time for the channel blockage scales and the flow rate, and inversely proportional to the concentration of particles of polydisperse suspension. The sorts of channel clogging, size exclusion, and subsequent deposition were associated with the distribution of particle size in the suspension.

Genovese and Sprakel (2011) assessed the effect of a single restriction along with the route on the flow and the microstructure of a dense colloidal suspension. The authors where able to assess the dynamic and static properties of colloidal suspensions using a microfluidic devicesand real-time imaging using confocal microscopy. Fluorescent colloidal particles with a diameter of 2.3 μm were prepared with a viscosity of 10 mPa.s at 25 ^{o}C, before being injected into the microfluidic device with a nominal volume fraction of 0.6. Due to steric stability with PVP polymer, the attraction of the Van der Waals between the particles has been reduced to a minimum. The microfluidic device had a range of 16 identical channels in parallel. It was found that the behavior of dense suspensions that flow through these channels was changed dramatically due to the existence of a sudden constriction in a microchannel.

A microfluidic technique was used previously by Sauret et al. (2014) to estimate the clogging by a small colloidal particle concentration. The colloidal suspension was flowed by a sequence of different cross-section microchannels to conduct the test. The purpose was to quantify the function of colloidal particles in the creation of blockages and the development of the filter cake. By measuring the time interval in an array of parallel microchannels between two clogging events, the concentration of particles with

a geometry selected for the microfluidic device can be estimated. The particles were coated with carboxylate groups to prevent the clustering and/or the attachment of the suspended particles on the walls of the microchannel. The range between 10^{-4} and 10^{-2} v/v was used as a volume fraction for the colloidal particles' suspension. The microfluidic unit was designed with a 190 μm inlet tube and 20 microchannels with a minimum width of 10 μm and a maximum width of 50 μm. Under the conditions of the experiments, the concentration of large particles, that have a diameter greater than or equal to the width of the throat, and the flow rate in the channel were the controlling parameters for the clogging dynamic.

The clogging conducted in parallel microtubes was examined by (Massenburg, Amstad, and Weitz 2016) using polystyrene beads, modeled on 10 parallel tapered microchannels using electrostatically attached colloids. Variable widths between 20 and 100 μm were used in model fabrication. At a volume fraction of 4%, monodisperse microbeads with a diameter of 3 μm were distributed. The flow rate through the channel array was evaluated during the experiment. The complete amount of particle size suspension passing through every channel before obstruction was measured in order to match the flow rate measurement when each channel was blocked. Consequently, the obstruction conduct relies on the geometry of the channel as well as on the shear-stress objects. It was found that the fluid flow rises through the constriction and leads to greater shear stress closer to the bottleneck. This greater shear stress prevents particles from being attached to the walls of the channel.

(Chen et al. 2017) considered the filtration capacity of a porous media and how it is affected by fines migration mechanisms, by investigating dynamic permeability. Three unconsolidated poorly cemented sandstones were applied under the microscope with three different grain size distribution. Fine quartz sand was poured with different

concentrations (10, 100, 200, and 500 ppm). The results showed with a wider particle size distribution, faster clogging and bridging were achieved in the system. Additionally, a very rapid bridging and clogging were archived with a higher concentration of particles. In the initial phase of the injection, a relatively rapid drop in permeability was observed, which decreased gradually over the course of the experiment.

Recently, Zhao, et al. (2019) fabricated a symmetrical microfluidic radial flow chip to examine the fine particle migration and clogging under radial flow. The chip consists of disc-shaped 'grains' of 300 μm diameter and 40 μm diameter pores. Glass particles with specific gravity of 2.6 and latex polystyrene particles with specific gravity of 1.05 both with diameters of 5 μm and 10 μm were used as fine particles with a mass concentration of 0.2%. The microfluidic chip was saturated with deionized water where the fluid was withdrawn using a peristaltic pump at a flow rate of 10 μL/min constantly. As result, for the latex and glass particle suspensions of 10 μm (o/d = 4), a few clogged pore appeared. While in the case of 5 μm latex suspension, (o/d = 8), some clogged pore constrictions gradually appear where no sign of clogging was observed when the suspension was prepared using 5 μm glass particles. The authors concluded suspensions including latex act as more effective clogging agents than glass-aqueous mixtures under equivalent experimental conditions.

2.1.3. Column-scale experiments on the mechanical processes

Moghadasi et al. (2004) presented the results of the theoretical and experimental study on the formation of damage mechanisms from invasion and deposition of fine particles into a porous media. They conducted their experiments using a column packed with glass beads with different mean diameters ranged from 245 to 1000 μm. Flow rates ranged between 12.5 to 200 cm^3/min,with suspension concentrations of spherical

aluminum oxide ranging between 15 to 2000 ppm. Their findings suggest that higher suspension concentrations result in higher rates of permeability damage. In addition, porous media with lower permeability have been identified as more susceptible to damage by fine particles. Smaller grain size resulted in a greater pressure gradient , indicative of lower permeabilities. At lower flow rates, the reduction in permeability occurred at much lower rates.

Khan et al. (2017) conducted modeling and experimental work to measure the changes in porosity and permeability, as an indication of formation damage. They examined the effect of fine particles size and concentration, as well as, the flow rate in modifying the structure of the porous media. The injected fine particles to grain size ratio, as claimed, were not covered in the previous research, where the investigation was performed on 10 and 40 (D/d) ratios. A CT scanner as well as pressure transducers were applied to measure the changes in porosity and permeability. Core flood tests at different flow rates of 40, 60, and 80 ml/min were conducted, with monodisperse glass beads with a 1 mm diameter was used as the framework particles. In order to predict the permeability reduction through porous media filtering, a combination of direct DEM and a network model at pore-scale was used. Five experimental test cases were applied with different flow rates and concentrations. The experimental results showed that the upper portion of the column experienced a large drop in porosity. As shown in Figure 2, the porosity was constant for all test cases around the 20 mm mark. Also, when the fine particles interact with the top part of the column, a very rapid reduction in permeability was initially observed in Figure.2. The later permeability change has a smaller slope, whereby permeability continues to decrease until injection stops. The lower part of the core shows a lower decline in permeability over the course of the experiment. It could be concluded that for lower particle concentration (1%), the initial

drop in the relative permeability at the top of the core was significantly higher. Also, under the same conditions a total clogging is noticed at the top of the core.

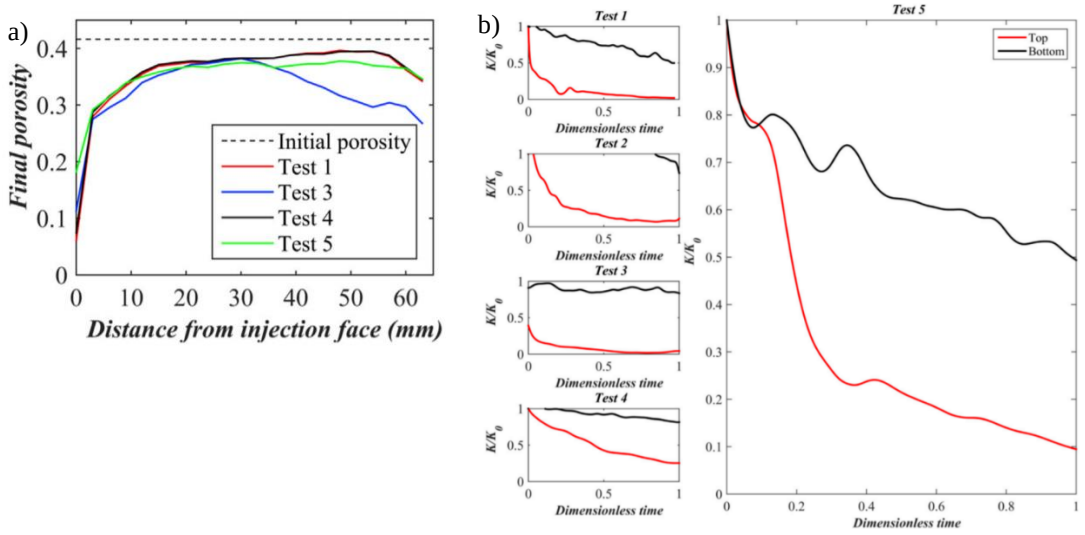

Figure 2 Formation damage due to fine injection observed in a glass bead pack experiment. a) Changes of porosity with distance from the inlet. b) Changes in permeability ratio as a function of the time (normalized) of injection. From (Khan et al. 2017)

Kim et al. (2017) carried out a similar experiment to verify the influence of fine particle size as well as the framework particles size and the speed at which the nanoparticles are transported in granular media filtration under conditions of treatment plants. Polyethyleneimine silver nanoparticles with spherical shapes and sizes of 10, 50, and 100 nm were used as fine particles, where a favorable condition for attachment was assumed by the use of positively charged particles with a negatively charged grain particles. As host particles, glass beads with different ranges were used in three different filter depths of 2, 4, and 8 cm. A constant flow rate was used for each solution to achieve the specified filtration speed with a fine influent concentration of 100 μg/L. greater filter depth, lower filtering speed, and smaller framework particle size were found to promote fines deposition. Decreasing the particle size of the filter from 0.776 to 0.325 mm has greatly increased the removal efficiency for all particle sizes. These results

were consistent with the theory that granular media particle size selection could be an influential factor in the removal of nanoparticles during filtration.

He et al. (2018) examined the effect of the emulsified vegetable oil (EVO) size in clogging pore throats and reducing the permeability during the bioremediation processes using column experiments. EVO is commonly used as an in situ anaerobic bioremediation stimulus substrate. The oil droplets were transported with the flow as colloidal particles once injected into porous media. Three columns were supplemented with medium and fine silica sand to serve as grain particles with different sizes of 0.25-0.5 mm and 0.1-0.25 mm. Two of the columns had a medium sand bead, where the nano-EVO was injected into one column and micron-EVO was injected into the other column. However, the third column was injected by nano-EVO and was filled with fine sand. Two piezometric tubes were connected to the inlet and outlet of the column to measure the permeability. Samples were collected from the outlet and analyzed to measure the COD concentration as an indication for the amount of EVO retained in the sediments. Results from column experiments show that the permeability of micron and nano-EVO was reduced by 20.4% and 3.2%, respectively. The retention of micron and nano-EVO in the porous media was 28.5% and 20.15%, respectively, in medium sand. EVO retention is, certainly, an important cause of loss of permeability, and reducing the EVO droplet size in porous media can effectively decrease the permeability reduction. The (o/d) ratio of nano-EVO and micron-EVO in medium sand was 1293.7 and 5.5 which explains the better piping of nano-EVO as compared to micron-EVO. The results also indicate that the larger the size of the colloidal particles, the higher the permeability reduction in the porous media. Furthermore, the retention percentage of the colloidal particles only was not enough to conclude the permeability reduction in porous media, however, it needs to be combined with the particles size.

Gao et al. (2018) studied the influence of coal fines migration on the pores of coal samples under various flooding conditions and fines concentration. Specifically, they investigated the generation and migration of coal fines in the field of coalbed methane production in the dewatering phase as an important unconventional gas resource. A series of flow experiments were conducted under field conditions with natural coal rock cores, where each experiment had a different concentration and flow rate of fines. The inlet and the outlet pressures in each experiment were analyzed to predict the permeability of the core. The equivalent permeability of the coal core samples with coal fine migration was calculated whenever the difference in pressure reached a pseudo-steady state. The impact on flow rate on the permeability in the coal cores was then analyzed and related to the migration of carbon fines. Six core samples with different gas permeabilities ranging between 0.02-0.46 millidarcy were used for the experiments. These demonstrated that the long-term preservation of differential pressure may result in new openings and severe fractures the coal rocks during the pure water injection; while coal fines may clog a few natural cleats and pores with micro cleat during their transport in porous media. Also, for the lower fine concentration, 0.004 g/cm^3, a lower reduction in permeability was observed, while a higher reduction in the core permeability caused by the injection of the higher fine concentration was observed. The authors concluded that maintaining a stable and effective depressurization rate during drainage can effectively limit the output of coal fines and decrease the damage to the permeability of coal reservoirs.

Recently, Saha, et al. (2019) studied the nano-zero-valent iron (nZVI) synthetization at a stable colloid (nano-sized) suspension with different levels of natural (Reetha extract) and two synthetics (PAA and Tween 20) surfactant, in a range of surfactant concentrations such as 1%, 2%, 5%, and 4% (v/v ratio) to evaluate the surface

charging effects on the size of particles. The efficiencies of the surfactant were compared to each other in terms of their ability to keep the nZVI particles in suspension in porous media. Two-column transport experiments were conducted using large and small sands as a model porous medium with sizes of 0.56 ± 0.015 mm and 0.22 ± 0.025 mm. Two different flow velocities of 2.3 and 4.82 m/h were tested in the column with large particles, while the flow velocities used in the small collector's size column were 0.36 and 2.3 m/h. Different pH was nZVI suspensions were used to determine the effect of pH and point of zero charges on the suitability of particles. The results concluded that surfactant with functional groups increases the electrostatic and steric repulsion on the nZVI surface which gives it ionic resistance to prevent aggregation of the particles and maintain the suspension of the fine fraction. The behavior of nZVI particles transport depends on different factors such as collector size, surface charge, and pore flow velocity.

2.1.4. Modeling and simulations on the mechanical processes

A population balance model was derived by Santos and Bedrikovetsky (2006) for the transport of particle suspension including the exclusion of solids by porous rock behavior. The model seeks to reduce the flow and accessibility to pore space, provided that large particles can not travel in smaller pores as they will be captured. Every particle has been assumed to only enter one pore. The pore space was locally modeled on a parallel bundle of capillaries. The flow-through each pore was proportional to the fourth power of its radius. For a single pore size medium, the analytical solution for the flow shows that small particles were captured advection free and that big particles do not enter the pore medium. As a result, in a pore medium with uniform size, there was no deep bed filtration. Also, the particles with a larger diameter than all pores did not migrate, while the smaller particles migrate without being

captured through the medium.

Bedrikovetsky et al. (2011) developed a new particle detachment mathematical model based on the matrix surface of pores based on the particles mechanical equilibrium. The classical theory of filtration assumes simultaneous capture and diffusion of particles. Results revealed that a dimensionless proportion was obtained between drag and normal forces that act on a particle that defines the torque-equilibrium. The maximum retention of the dimensionless ratio (dislodging number) closes the mechanism of control of colloid transport equations with the release of particles.The highest maintained concentration compared with the dislodging numbers closes equations system with particle dislodging for deep bed filtration. An exact analytical solution was possible with the single-dimensional suspension problem injecting into a clean bed. The solution includes an erosion front that meets the torque balance criterion. The novel characteristic of the solution was that the erosion front has a small discontinuity. The solution demonstrates that erosion begins at the core inlet and extends into the core until the torque balance zone is at the entire core; particle suppression no longer occurs from that point. The solution allows the determination of all three model coefficients of pressure drop curve during steady flow injection (filtration and formation damage coefficients together with the peak retention concentration).

A deep bed filtration model for migration of the associated surface phase was developed by Yuan and Shapiro (2011). The authors suggested a mathematical model for suspension/colloid flow in porous media and non-monotonic deposition. The movement of monodispersed solids in the bulk aqueous phase was presumed to be described by the advection-dispersion equation with a single sink term and a source term. The model considered one-dimensional flow as it was prevalent in most studies

and many applications. The model parameters estimation was performed with available experimental information from previous studies. The sensitivity analysis of the generated model reviled that the greater the ratio of advection velocity of particles in the surface associated phase to advection velocity of particles in the bulk aqueous phase, represented by f_m, leads to maximum final deposition closer to the inlet. The larger the dimensionless longitudinal dispersity values represented by R in the mass aqueous phase, the closer the peak of final deposition will occur to the outlet. However, this behavior was also associated with mass aqueous transport where more dispersivity values will cause the breakthrough curve to be washed out more than expected. The results of the numerical modeling were in agreement with the experimental observations.

The movement of fine particles in porous media was investigated by Hirabayashi et al. (2012) to explore its impact on suspension permeability at the micro-scale level. A solid-liquid two-phase Lattice Boltzmann Method with spherical sand grains of distinct diameters enabling 3D microscopic numerical simulations were used. The results indicated that the change of the pressure over the distance was observed to be linearly proportional to the relative velocities between the fine particles and the fluid. though measurement of the relative velocity not possible. The study suggested that the proportion of particles trapped in the porous media to the mobile particles can be related to the relative velocity of particles and their size in relation to the framework particles. Moreover, the decrease in apparent permeability relies substantially on the size and concentration of the mobile fine particles.

Boccardo et al. (2014) studied particle transport and deposition in different pore network geometries and flow rates under favorable collector-particle interactions using microscale CFD simulations. The results indicated that the porosity and effective grain

size were capable of fully characterizing the observed behaviors in the case of circular collectors, while in the case of realistic porous media, another parameter should be included in the laws predicting Brownian particle deposition. However, hydrodynamic forces were neglected which limited the ability to study the influence of large particles on drag forces.

Lei et al. (2017) studied the effects of concentration and density of suspended particles on their deposition at the interface of porous media. Using the direct-forcing immersed boundary-lattice Boltzmann (IB-LBM) method, the migration, and deposition of micro-particles was simulated using different densities of 2, 2.45, and 3 g/cm^3 and different concentrations of 13.9, 18.5, and 23.1 particles/mm^2. A proportional relationship was obtained between increasing particle density and the number of particles deposited on porous media. The micro-particles easily move over interfaces when the concentration of suspended particles was small and the deposition at the interface was larger. Therefore, the concentration of particulate was not strongly correlated to the overall quantity of deposition but impacts the distribution of deposited particles.

Li and Prigiobbe (2018) conducted pore-scale numerical simulations to investigate fines migration and its ability to trace the behavior of a single particle. The model was composed of three components: (1) Lattice Boltzmann method (LBM), (2) immersed boundary method (IBM), and (3) discrete element method (DEM). Findings from this study reveal that although fine particles decrease the permeability, original permeability can be restored through the application of a high-pressure drop. In addition, the main two factors governing the migration process of fine particles were the size of fines and the geometry of pores.

Su, et al. (2019) presented a direct numerical simulation for particle flow in

porous media. The movement of the fluid into the pores was described using the Navier-Stokes equation. The discrete element method was used for describing the contact between fine and grains particles. ERIGID was used to detect the contact between the particles and the pore walls. The fictitious domain method was used to evaluate fluid-particle interactions. The base point-increment method was used to enhance the numerical accuracy of the discrete element method. The time coupling between fluid tracking and discrete element method was realized by a dual adaptive time-stepping scheme. The pore structure was reconstructed from real rock samples using micro-CT images. The results indicated that particle clogging causes changes in local pressure, reflected by changes in the pressure difference between the inlet and the outlet. These pressure differences can lead to fluid velocity fluctuating in the pore space, which can influence particle motion in the affected area. Also, particle size plays an important role in their migration, where small particles migrate along the mainstream direction and are less dispersive along the flowing direction.

Numerically, the influence of the distribution of particle size on contaminant transport in porous media by Won et al. (2019). The model utilized a lognormal distribution to describe the distribution of particle size. In addition, simulated breakthrough curves were determined to evaluate bed efficiency and the contaminant saturation and the experimental results on the contaminant sand and the contaminant Colloidal particle reaction model were provided and validated. The colloidal particle-sand interaction during the transport in saturated porous media was taken into consideration by three major processes namely, straining, attachment, and detachment. For a sampling of colloidal particles and sand during certain particle size ranges, the Latin Hypercube Sampling (LHCS) technique was used. The results indicated that, as the average size and the standard deviation in colloidal solids increased, the transport

of contaminants was delayed. With the enhanced average size of colloidal particles, the effects of a standard deviation on retardation of transport became more significant due to the median size and standard deviation in the quantity of the retained colloidal particles. Therefore, in the prediction of contaminant transport, the particle size distribution should be considered.

2.2. Chemical processes of fines in porous media

2.2.1. Theoretical studies on the chemical processes

The fabric of fines or the degree to which fines cluster together can have a substantial impact on the behavior of the fines in the porous media system. In general, the gravitational influence is weak when the particle size is less than 1 μm or if the specific surface is larger than 25 m^2/g and the electrical force controls the cluster or fabric of the particles. The clustering behavior of the fines depends on the chemistry of the water, particularly, the ionic strength and pH.

Bulkier particles of silica have weaker and more homogeneous distributions of the surface load than flat particles i.e. phyllosilicates. These bulky particles with similar superficial loads did not cluster in freshwater but are more likely to remain dispersed and participate in migration of piping type. The recharged particles in salty water, however, can cluster because positive ions interact between these particles in the surrounding water, resulting in decreasing their repulsive inter-particle forces. The model Sogami-Ise is based on coulombic forces between similar charges and different charges. In an ionic fluid, such as brine, the coulombic repulsion can be balanced against ions in the fluid between such particles, reducing duple layer repulsive forces and cause attractiveness between the neighboring particles (McBride and Baveye 2010; Mojid and Cho 2006; Sogami and Ise 1984). Clustering is usually occurring in freshwater where the double layer is thick and minimized for these particles. As the

concentration of salt increases, the thickness of the double layer decreases, allowing particles to easily cluster and build bridges and blockages on the pores (Jang et al. 2018; McBride and Baveye 2010; Molnar et al. 2015).

2.2.2. Micro-scale experiments on the chemical processes

Auset and Keller (2006) conducted several experiments for various particle dimensions, grain surface roughness, ionic strength, and flow rates. Tracking of path and destiny of individual colloids using an optical microscope was used to observe and measure straining and attachment. A spherical polystyrene latex particle was used as a synthetic colloid. The ionic strength of the solution was adjusted by adjusting the concentration of KCl concentration. The experiments have been performed in physical micromodels that contain a homogenous pore network model. The colloidal particles strained at the first 1 to 2 pores of the porous media, while the attachment took place to form the inlet to the first 6 to 10 pore spaces. The likelihood of attachment was considerably decreased once a particle crossed the initial area. The attachment was anticipated to take place further upstream in a longer medium but at lower rates than in the first few pores. The roughness of the grain surface can be very crucial in determining the effectiveness of colloid collisions. With the roughness of the porous media, collision efficiencies improved by a factor of two to three. The impact of grain roughness on filtration could be explained by a grain shape factor that could be added to the collector efficiency equation. Collision efficiencies have risen with enhanced ionic strength solutions. Wyss et al. (2006) concluded that the time scale relies on the length scale sensitively of the repulsive interaction between particles.

Colloidal particle deposition in hydrodynamic fluids on a solid surface has been investigated by Unni and Yang (2008). In different physiochemical conditions, micro-scale studies were carried out using several parameters including particle size, Reynolds

number and electrolyte concentration. The test results were compared with a statistical model for phenomenology to evaluate the particle deposition in a parallel microchannel from pressure-driven flows. Two different sizes of polystyrene latex particles were used in NaCl electrolytes of different concentrations with a particle concentration of $2x10^{14}/m^3$. Their findings demonstrated that particle deposition was significantly affected by the electrolyte concentration, which can be explained by EDL interactions between charged particulate matter and collector surfaces. A rise in the ion concentration would reduce the EDL thickness and zeta potential of the particle surface. In fact, due to the rise in the thickness of the border layer downstream of the channel, fewer particles exist in the area of the channel wall downstream compared with those in the upper stream due to the shrinking of the particle deposition flow. It was also clear that the smaller the particles, the higher the effect of the surface charges on their behavior.

The dynamic accumulation and deposition of particles within porous media was investigated for latex suspensions by Agbangla et al. (2012). The authors examined the behavior under distinct particles concentrations, suspension flow rate, the density of the particles, and fluid physical-chemical conditions. The findings indicated that clogging is attributable to different factors, such as latex particle volumetric concentration, suspension flow rate, and physical-chemical conditions. When colloidal particles are within ultra-pure water or salt solution, the shift to cluster formation seems to be under the same conditions. The results also verified that a critical flux density was presented that leads to the accumulation of particles and to clogging of the micromodel. Also, increasing the concentration of particles in high salinity water leads to an increase in the clustering of particles, as well as increasing the flow rate.

Dersoir et al. (2015) studied the clogging of a single-pore microfluidic filter

to determine the effect of hydrodynamics and the DLVO forces on clog formation. The impact of the pore geometry on the clogging structure, as well as the hydraulic conditions and the ionic strength of the solution, were investigated. The colloidal particles used had diameters ranged from 1-10 μm and it was injected with a volume fractions ranging from 10-1to 10-5. The observation indicates that when the pressure increases, the pores were blocked faster because the number of particles flowing through the pores was equivalent to that of the particles needed to create such clogging faster. Moreover, when ionic strength rises, the number of particles needed to create clogging decreased significantly.

Argent et al. (2015) investigated the influence of nanoscale surface roughness on particle retention in porous media under favorable chemical conditions (i.e. high ionic concentration). They visualized and described the process of particle retention on a physically heterogeneous solid surface, taking into account the impact on retention processes of solution chemistry, surface roughness, and particle size. Under various chemical conditions, a glass micro-model was used to visualize the particle retention and its spatial distribution on the glass surface. It was shown that, if the concentration of the solution was high, the strength of the primary minimum attachment was reduced considerably by the nanoscale roughness on solid surfaces. The increase of roughness fraction on the solid surface-enhanced primary minimum strength, whereas the increase of roughness height reduced the strength of minimum primary interactions. The results demonstrated that, for surfaces with high roughness, only a fraction of solid surface was available for particle retention even at a very high IS of 0.6 M.

Robert et al. (2016) investigated the impact of hydrodynamics and colloidal interactions on colloidal accumulation that result in the mechanical, structural, and geometrical modification of dense structures in porous media. The interplay was

explored by adjusting the flow pattern and ionic strength with model suspensions which flow into a microfabricated porous obstacle. There were two different obstacle forms: firstly, a single pore consisting of two elongated collectors with a gap of a thickness of 10 mm and spherical caps at the end. The second form was a sheltered pore with three single parallel pores with a triangular barrier placed at a variable range upstream to adjust the shear magnitude. These two forms enable velocity gradients to be modulated and, therefore, high and low-shear accumulation schemes to be considered. By adding NaCl, the ionic strength has been enhanced up to 50 mM,below the critical coagulation concentration of 70 mM. Suspensions were then injected over a range of 5-500 μL/min. Four different aggregate forms were recognized based on the flow represented by the Peclet number and the ionic strength conditions. The strong electrostatic repulsion forces prevent particles from binding in low ionic strength conditions. Therefore, under these conditions, the aggregates formed were not cohesive and only maintain stability through the force of the flow. The corner form also corresponds with the velocities close to the pores in single pores. Therefore, when particles have no contact, this sandpile-like form was anticipated and recovered in the 'labile' area of the stage. The screening of the electrostatic repulsion makes it possible for irreversible particle attachment to form cohesive aggregates.

The interplay between hydrodynamic and physicochemical interactions that affects the micro-particles filtration was investigated using microfluidic devices with real-time pore visualization by Sendekie and Bacchin (2016). The dynamics of clogging and changes in permeability were evaluated with respect to time by monitoring both flow rate and pressure difference. Flux stepping tests were conducted under various physicochemical conditions to determine distinct clogging scenarios. Filtration studies were carried out using a microfluidic flow control system under steady

pressure and steady flow rates. Suspensions consisted of 5 μm diameter latex polystyrene microspheres . Three primary tests were conducted, known as, flux steps, steady pressure, and steady flux tests. No particle clogging associated with poor collision efficiency was noted at a low flow rate in the presence of potential barriers. A higher stream rate induces the impulse impact between particles, which leads to solid arches at pores. The association of elevated flow rate and elevated ionic strength demonstrated that the filtering method was dominated by the shear strength of the clogs which leads to regular archery sweeps that can delay clogging. It could be concluded that higher flow rates provide enough energy to the particles to collapse and cluster at high ionic concentrations.

Cejas et al. (2017) used microfluidics to investigate the deposition of Brownian particles in a low Reynolds number flow. The authors focused on the specific case of high salinity, evaluating the role of electrostatic forces. Straight channeled microfluidic devices were used to analyze thousands of discrete particles with controlled surface chemistry and flow conditions. A suspension of unmodified polystyrene commercial monodisperse particles with 5 μm diameter was used as a liquid. The retention profiles decrease with the inverse of the square root of distance from the inlet.

Yu et al. (2018) studied migration of fines in real rock volumes using micro-CT experimental imaging A single-phase flood test was performed on a Berea sandstone core plug where fine particles were injected inside the core. A dry scan was captured prior to the flood. The plug was then saturated with 4%NaCl solution with a a flow rate of 3 ml/h before being flushed with fresh water. During these experiments, the difference in pressure through the core plug was monitored and particle counting via Electron Microscope-EDS (Energy Dispersive Spectroscopy) imaging were employed to assess fines concentration inform the produced water. After the flood trial, the plug

was reworked and the second image with the first to measure fines migration was matched. Porosity and initially measured core permeability were 24.3% and 1560 mD, respectively. Results indicated that micro CT imagery was capable of investigating formation damage (permeability reduction) due to fines migration. Injection of freshwater resulted in a sharp rise in the production of clay components. The resolution of the sand-phase fraction was not changed, although both the high-salinity and freshwater injections produced sand. Clays were mobilized during the injection at the end of the center plug. At the end of the development of the core plug, some of these transported clays are loosened. Computations performed on a tiny micro-CT image sub volumes did not indicate any damage to permeability, but calculations performed on a larger sub volume showed a decrease of 50%. This demonstrates that the production end of the core plug was damaged due to clay fines straining.

The progressive blockage of pores at the particle scale was considered by Dersoir et al. (2019), who attempted to characterize the clogging process under different conditions, pertaining to hydrodynamics, confinement, and physical chemistry. They concentrated on an intermediate degree of containment (o/D ratio), for which very few particles were in theory needed to block the pore throat which had a height of three times and a width of four times the diameter of the particles. The pore walls at pore corners capture separated particles at the start of the procedure. It was noted that within the pore, there were only two to four isolated aggregates, which first develop separately and then combine. Because of the colloidal particles' high surface charges, these aggregates first develop along the stream path, before they also reach the middle of the pore, which blocks the pores completely.

2.2.3. Column-scale experiments on the chemical processes

The impact of colloidal particles shape on filtration rates in porous media was

examined by Salerno et al. (2006) by measuring the retention rate in packaged beds of different particles with distinct aspect ratios. Spherical polystyrene latex microspheres were used as colloidal particles. These particles were injected into packs of 40 μm diameter glass beads in aqueous phases with two ionic strengths of 1 and 100 mM. In proportion to their aspect ratios, the retention rate and the collision efficiency of the three distinct kinds of particles rose considerably, showing that rods shape particles are preferentially retained when compared to spherical particles. Solution chemistry was a significant factor in particle retention. The higher IS solution showing a greater rise in collision efficiencies for prolate spheroids. The exposed surface of the particle-packed bead interaction rises or reduces in comparison with that for spherical colloids depending on the side or tip interaction. For IS of 100 mM, the interaction is always appealing and short, and therefore it is probably that the surface area factor is not essential. Calculations for a 3:1 aspect ratio show that the efficient region of interaction reduces to 20 kT, but still high enough to prevent contact, while adhesion still happens.

Sharma et al. (2008) conducted colloid mobilization experiments under different boundary conditions, by infiltration of unsaturated sandy sediment columns. In addition, experiments with flotation in the form of colloids in the bulk fluid and at the liquid-gas interface were measured separately. The transportation mechanisms were examined using force calculation (adhesive and interfacial forces). Through mobilization experiments, aqueous solutions have been infiltrated into the packed sediment columns at various flow rates and different ionic strengths. Deionized water was infiltrated at different flow rates to assess the effect of flow rate on colloid mobilization. To evaluate the effect of ionic strength on colloids mobilization, one flow rate was chosen (0.071 cm/min), and the ionic strength of the influxes was adjusted to match ionic strength of 3, 30, 300, 1500, and 3000 mM. The colloid concentration in

the effluent was measured through turbidity measurements using a 300 nm wavelength. Results showed that the amount of colloid mobilization was different under suction-controlled conditions. The shape of the colloid breakthrough curves was different between the boundaries. Results showed the importance of liquid-gas interface interfacial forces in the mobilization of colloids. The maximum colloid levels increased in the outflow by a factor of five to six, with both the drainage boundary and the suction boundary tests increasing the flow speeds from 0.018 to 0.284 cm/min. Raising the ionic strength of the infiltration solution resulted in a decrease in the concentrations and overall colloid mass, which implies further retention under both drainage and suction conditions.

The effect of the shape of colloids on their retention and release in saturated porous media was also investigated by Liu et al. (2010). In water-saturated glass bead columns, colloids were injected into deionized water and an electrolyte solution with 0.2 M as ionic strength. The carboxylate modified latex colloids with a diameter of 500 nm and rod shape with an aspect ratio of 7 were used as the particles. Both hydrophilic particles have the same volume and density with negative charges. The model of grain host particles used was glass beads with a medium grain size of 0.22 mm. Colloid concentration in the tests for spherical particles was 10 mg/L and rod particles were 0.5 mg/L. Spherical particles were mainly deposited with secondary minimum retention, whilst rod shape particles had been deposited with primary and secondary energy minimums, which was linked to colloid electrostatic characteristics and a preferred orientation with respect to the host particulate.

Column experiments have been carried out by Liu et al. (2016) to analyze the effects of the hydrodynamic and hydrochemistry conditions on the transport of humic acid colloidal particles. A suspension was prepared to better regulate the simulated

recharged water's hydrochemical properties. These conditions were simulated by the influential suspension in distinct conditions. Column studies were performed to examine the transport of humic acid colloidal through glass beads under various pH, cation valence (Na^+, Ca^{2+}), ionic strength, and flow rate. The results showed that colloid transport can be improved substantially when conditions favor less deposition. When the pH increases from 5 to 9, the peak concentration increases as well from 0.98 to 1, indicating a slight improvement in colloidal transport. The transportation of humic acid colloids was also influenced by IS. As the IS increases, electrical double layer thickness reduces, and the repulsion between colloids and collectors will be reduced as well, resulting in a decrease in the effluent concentration of colloids. Transportation considerably improved as the flow rate increases because of the equilibrium of forces between the colloidal particles and the porous medium.

Russell et al. (2017) investigated the kaolinite content in rocks and its impact on permeability variation during low salinity enhanced oil recovery. In six sand packs with distinct kaolinite content ranging from 0 to 10 weight percent, a sequence of injections was conducted with decreasing salinity. Studies were carried out using unconsolidated sand packs consisting of silica sand as host particles and kaolinite particles. Seven distinct solutions of sodium chloride were sequentially injected with deionized water. These experiments showed that higher kaolinite fractions reduce the sand pack initial permeability. This observation was most likely due to attaching kaolinite particles to the rock to coat the pore throats under a higher concentration of kaolinite. Also, the reduction of permeability was greater after the injection of freshwater in higher kaolinite content cores due to large pore radii connected with high levels of kaolinite, which increases the staining intensity, thus, increase the permeability reduction. The rise in permeability occurs in high salinities where the re-

attachment is more intensive. At low salinities, the possibility of re-attachment was small and, thus, the increase in permeability occurred due to detachment of particles was dominated by permeability decline due to straining.

Tan et al. (2017) conducted multi-temporal observations on intrusion and refreshing of marine water using column experiments with a coastal soil based on natural flow conditions. Colloid and associated heavy metal transport under different IS and pH was investigated. Also, the development of colloid size distribution, colloid migration, and hydraulic aquifer parameters at various phases of interaction between seawater and freshwater was examined. Results concluded that colloid immobilization caused a higher background concentration of heavy metals. However, based on their reliance on seawater-freshwater cycles, the release and deposition of colloidal particles dominate the transport behavior as the IS and pH changes. Meanwhile, heavy metal transportation was determined based on carrier-colloid behavior, particularly for heavy metals with powerful affinities, such as Pb. The reduction in the overall surface area of migrating colloids probably led to a reduction in heavy metal transportation related to colloids.

Sadri et al. (2017) examined the impact of the surface characteristics of collector beads on the transport of colloidal particles in porous media. The dynamics of deposition and the accumulation of colloids in contact with the soda lime glass collector particles was investigated. The evaluation of colloidal particles and their aggregate concentration in columns packed with glass beads was performed using time-resolved dynamic light scattering (TR-DLS) and ultraviolet-visible (UV-V) spectroscopy. Results indicated that ions released from the collector's surface cause colloidal particles to aggregate. The aggregation and removal of colloidal particles did not dominate the transport behavior in the lack of surface ions which facilitated colloid transport.

Li et al. (2018) investigated the transport properties of high colloidal heterogeneous $Mg(OH)_2$ concentrations in porous media using column experiments. The influence on the transport properties of colloidal $Mg(OH)_2$ was analyzed under several parameters. Several experiments were performed with different flux velocities, porous media sizes, ionic strengths and initial colloid concentrations. River sand was used as grain particles with five different sizes ranging from 0.115 to 0.53 mm. A total of 15 experiments were carried out with different flow rates (between 0.158 and 1.23 m/h), various ionic strengths (between 0.3 and 2 mM), and different $Mg(OH)_2$ concentrations (5 to 10 mg/l). Calculus methods combined with the Colloid Filtration Theory, T-E equation, and modified Maxwell theory were used to model the transport of high concentrations of the $Mg(OH)_2$ colloid. Results indicated that C/C_0 was independent of the initial $Mg(OH)_2$ colloidal concentration, suggesting a linear relationship between the deposition of the particles in porous media and the initial colloidal concentration. Also, the higher flow rates resulted in a greater hydrodynamic forces that increased the colloid detachment from the studied porous media and increased the effluent concentration, as confirmed by Shen et al. (2010). The increase in porous media size would reduce hydrodynamic strength significantly and decrease colloid detachment from porous media. However, since the porous media size was negatively correlated to collision efficiency, larger pores within a given porous media could reduce the efficacy of collision. Hence, the impact of porous media on colloidal $Mg(OH)_2$ migration was not as important as the flow rate Torkzaban et al. (2007).

Kanimozhi et al. (2019) conducted laboratory experiments for saline water injection in the presence of kaolinite colloidal fines in high-temperature carbonate porous media. Three sets of core flood tests conducted at 100, 150, and 200 °C were performed. At these temperatures, kaolinite suspended in water was introduced into the

core, to examine possible hydraulic damage or decline in permeability. The increase in pore volume injection (PVI) was noticed to improve the concentration of fines. Higher temperatures (200° C) also contribute to the elevated level of kaolinite fine concentration, because at greater temperatures, the fine particles were excited. After some time, the permeability of the core decreased because of fine suspension and straining. The higher loss in permeability was recorded at a higher temperature at 200 °C.

2.2.4. Modeling and simulations of chemical processes

Li et al. (2010) examined the sensitivity and effects of solution chemistry, fluid velocity, and grain and colloid size to simulate colloid deposition in the discretization of pore spaces. Lattice-Boltzmann flow simulations have been carried out in two packaging systems at different discretization resolutions. Simulated flux fields were incorporated in both models to analyze colloid transport in a three-dimensional particle tracking system. In the unit cells of the simple (SC) and dense packaging (DC) schemes, the susceptibility of the virtual colloid deposition to porous space discretization was tested. Both structures include grain connections, which are usable in real porous media. Porosity structures 0.476 and 0.26 are simple cubic and dense packing structures. Force and torque balances have been used to assess the colloidal velocity within the pores. Simulations of particle transport(?) show that colloids can be preserved in favorable as well as unfavorable conditions for deposition. A large proportion of deposition (5-15%) occurred at contacts between grains with a colloidal-grain ratio of greater than 0.01. At lower ratios and low flow rates, grain-to-grain contact deposition was negligible. Under the low energy barrier criteria, the differences of total deposition between the medium and lower fluid velocities were at least 5% of both packing systems for colloids with diameters of less than 1.0 μm and grain diameter of 300 μm.

A laboratory-based mathematical model for fines migration was introduced by You et al. (2016) to predict the reduction in productivity during exploitation of geothermal reservoirs. Water flow rate in the mass equation was substituted by particle velocity, which explains long periods for the stabilization of the permeability of the mobilized particles by slow surface movement. To explain its non-convex shape, the highest retention function for a monolayer of size-distributed fines was also implemented in the fundamental equation. The exact solution to the system of one-dimensional fluid equations with a steady increase in velocity was achieved. The velocity of migrating particles was supposed to be different from that of carriers. In comparison with their advection, the dispersion of fine particles was also insignificant. Due to the segregation of the particles, an insignificant rise in permeability has been alleged in comparison with the reduction due to particle strain. The analytical model for the mobilization of fines, migrations, and pressures provides explicit formulas for suspended and strained concentrations and core permeability. Slow-motion of released rolling or sliding particles can explain the large stabilization periods during fine migration where the implementation of the Driving Delay Factor enables identification of permeability history. Modeling predictions for geothermal conditions at high temperatures show that the maximum retention concentration reduces when compared to conventional aquifers and petroleum reservoirs, resulting in more serious permeability damage. A good balance has been noted between the measured permeability of the laboratory and the model.

Kheirabadi et al. (2017) developed a one-dimensional numerical model using a fully implicit finite difference method for colloid-associated contaminant transport. This system was based on equations of mass balance and mechanisms of mass partitioning between solid matrix and carriers, as well as, contaminants and liquids.

Two approaches represent this phenomenon: a fully kinetic first-order approach, and equilibrium approach. The formulation of the model can be simplified by applying the equilibrium distribution of particles. In practical cases, however, contaminant transport can be predicted more accurately by kinetic simulation. The effect of numerous chemical and physical coefficients on the movement of pollutants was investigated to determine the model's vulnerability. When contaminant sorption is in balance, mass transfer rates of adsorption and desorption by mobile and immobile colloids were similar. Contaminants were shown to be transported over larger distances than traditional advection diagnostic models (Figure 3). According to this work, a drop in the coefficient of colloidal deposition will substantially increase the overall transport of mobile pollutants.

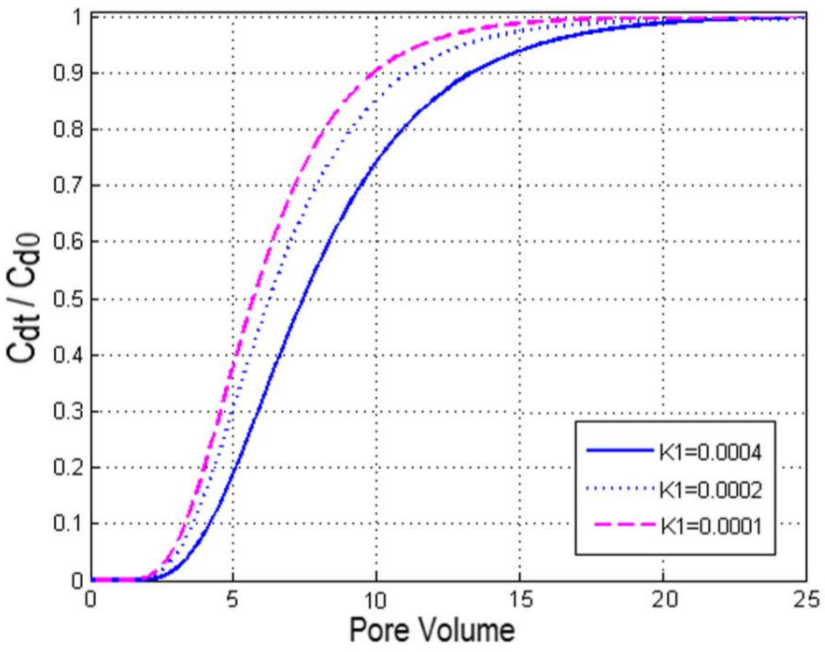

Figure 3: Sensitivity of the kinetic model of Kheirabadi et al. (2017) to changes in adsorption rate. From (Kheirabadi et al. 2017)

Yang and Bedrikovetsky (2017) derived an exact solution for arbitrary filtration, accessibility, and drift-delay-functions on fine migration problems. The solution-derived forms of curves demonstrate the varying colloidal suspension flows

between linear and nonlinear. The exact solution distinguishes between fines-migration flows between uniform profiles for hanging and retaining concentration before the front and no hanged fines behind the front. The model represented the transfer and preservation of fine particles by low-salinity water injection into porous media. The retention rate was commensurate with the advective particle. Fine-particle dispersion was negligible as opposed to particle advection. Suspended particles were also assumed to be mono-sized. After the injection of several pore (volumes?), (fines?) concentration and pressure drop throughout the core stablizes. Modeling of Navier –Stokes suspension-colloidal flows within porous media also demonstrates that the particle flow close to the pore wall was significantly smaller than that of theinjected fluid velocity. It is assumed that the suspended particluate fill the pore space at the start of the injection and are yet to be captured by the framework. It was also assumed that the associated fines will be released immediately preceding a change in salinity. A retention mechanism was assumed, where parameters changing porous space and capture probability are determined by the retention concentration. The solution demonstrates that the colloidal concentrations of suspended and retained particles ahead of the concentration front depend only on the time. The concentration suspended behind the front was zero, and the retention was constant. Moreover, the lower the ionic strength in the injected water, the lower the average retention concentration regardless of the anion type.

Coronado and Díaz-Viera (2017) presented a model to describe fine migration, detachment, and blockage, and the impairment of permeability observed in low-salinity single-phase laboratory core flood experiments. The key principle of maximal (critical) preservation was retained, but a physically unrealistic abrupt cut-off from the attached fine was present. An updated fines equation was considered, and the peak retention

function was a more general mathematical expression. The updated equation describes the smoother kinetics of the fastener-removal process and extends the overall retention function to low critical salinity concentrations. The equation scheme has been numerically evaluated using the finite element method and applied in three studies of low-salinity water injection. A cylindrical sandstone core saturated with saline water was used as the model domain. Initial permeability and porosity in the core were assumed to be constant. The brine was constantly injected into the inlet face of the core during the injection experiment, while the pressure was constantly maintained in the outlet face. The balanced equation for the fines involves mobile fines dispersion and the sink-source terms of the attached/detached and strained fines. Results showed that for water injection with salinity lower than 0.05%, the attached fine concentration remains constant and then starts to decrease gradually at PVI of 400. The authors concluded that the attached fines were almost uniform inside the plugs, although they have decreased in time. The behavior of the blocking fines was explained by the concentration of which depends on PVI for 3 places in the plug. No fines were clogging at the plug input and the number of clogged fines increases over time (i.e. PVI) and with distance inside the plug.

Russell et al. (2018) presented a mathematical model for fines in single-axial coordinates describing the kinetics of particle detachment separately due to variations in velocity and salinity. A system of transport equations with particle detachment kinetics, where the high-speed detachment was immediate because of the flow incompressibility and the detachment by decreasing the fluid salinity was delayed due to the micro-scale diffusion. The fluid, as well as the particles, were considered to be incompressible. Particles suspended were supposed to travel at a lower velocity than fluid velocity by a drift delay factor across the porous space. The straining of particles

was assumed to be an irreversible process. The attachment of particles due to the electrostatic attraction was ignored. A postponed impact on the detachment of particles was assumed to have changes to the fluid salinity by changes in NaCl concentration. The strain rate was expected to be proportional to the incoming concentration of the suspended particle. The attached concentration was governed by the critical retention function based on fluid salinity and velocity. It was predicted that particles mobilize immediately at the start of high-velocity injections, while mobilizing gradually behind the low-salinity front performed deep bed filtration independently.

Chequer and Bedrikovetsky (2019) developed a set of governing equations that describe fine particle transport in undersaturated and oversaturated rock. In laboratory tests, the critical velocity and salinity were identified, enabling a controlled oversaturation and undersaturation during the core flooding. 1D suspension-colloidal transport was studied using a mathematical and laboratory model for over and undersaturated fines. For suspension colloidal transport with fine detachment and retention in porous media, the following assumptions were used for the modeling: carrier fluids were incompressible and the concentration of fines was low, to avoid the influence on carrier fluid volumes. The effect of porosity and particle mobility were considered negligible. The kinetic equation describes the strain rate of the particles and is proportional to the particle flux. A comprehensive system of single-phase flow equations account for the fines migration due to the alteration in the salinity comprises of the mass balance equation for the concentrations of the different types of particles; strain kinetic rate, maximum retention function for attached concentration, salt mass balance, and modified Darcy's law accounting for permeability damage. In the oversaturated case, at the early stage of injecting, the excess of the initial concentration attached over the critical retention value was released. When the injected salinity

exceeds critical salinity in the undersaturated case, no fine mobilized movement was caused by low-salinity water injection. The pattern in the flow in the oversaturated case was fines from the start of the injection, corresponding to the immediate release of fines at the beginning of the injection and their deep bed filtration. For the under-saturated case, the pattern was the fact that the fines will not appear until critical salinity is reached in the core effluent.

Modern pore-scale modeling has been developed by Sanematsu et al. (2019) to simulate the fine particles transport in realistic porous media at the pore-scale using X-ray microtomographic images. The fluid and particle transport was simulated using direct numerical simulations of fundamental motion equations. Stokes flow and particle tracking using the Lagrangian method was used to track the transportation and fates of the nanoparticles. X-ray microcomputed tomographic (μCT) images from Berea sandstone were used to determine the effect of particle diameter and compute domains consisting of attractive and dramatic surrounding forces and flow rates. The incorporation of surface forces by a modular arrangement that permits the inclusion of various surface force profiles through the porous medium has resulted from tabular or theoretical data together with the unstructured grid. Results revealed that the rise of the initial surface force profile induced a rise in particle deposition in the presence of favorable surface forces respectively. The susceptibility to changes in surface forces was improved by smaller particles. The flow rate had an important impact on the recovery of colloidal particles when attractive surface forces were present.

CHAPTER 3: NUMERICAL MODEL STRUCTURE

3.1. Geometric representation of porous media

Synchrotron x-ray micro computed tomographic images of the studied sediments were captured at the Argonne National Laboratory (ANL) synchrotron facility (Jarrar et al. 2018). 2D sections (orthoslices) were taken from the resultant volume images which were subsequently binarized. A MATLAB code was used to extract the grain particles boundary out of the segmented images by creating small line segments when the gradient value between two adjacent pixels is non-zero. The line segments were converted to polylines in AutoCAD. The pore structure had to go through a post processing steps, since pore throats were lost when scanning the sediments. Hence, the pore throats were edited to have a more representative geometry. The extrusion command was used after that to add depth to the extracted boundaries creating a quasi 2D extruded geometry. This geometry was converted to a mesh and used directly for the DEM model calculation. Additionally, the geometry was used to create the fluid domain mesh for the CFD model. Figure 4 illustrates the geometry creation workflow described above.

The fluid domain mesh was created and enhanced using the built-in libraries in OpenFOAM. The features of the solid's geometry were extracted using SurfaceFeatureExtract tool. This process involves simplifying the geometry by only including edges/features whose angles exceed a determined value for computational simplification. Then, features were used to create the hexahedral mesh that represents the fluid domain. This process starts by encompassing the entire domain with a background hexahedral mesh using BlockMesh, then further refinement is done to fit the solid's geometry using SnappyHexMesh. The refinement was done to be of multiple levels to ensure both the minimization of computational complexity, as well as the

accurate representation of the fluid domain. The refinement works by starting from a specific point within the mesh and splitting the hexahedral background mesh elements to capture the details of edges. Then cells that lie within an enclosed bounding region in the domain are removed. The remaining cells' vertex points are then moved to snap to the geometry's surfaces to eliminate the jagged edges. This step ensures accurate representation of the fluid domain by discretizing it to smaller volumes that will be used to numerically solve the mathematical equations of the fluid flow (Figure 5).

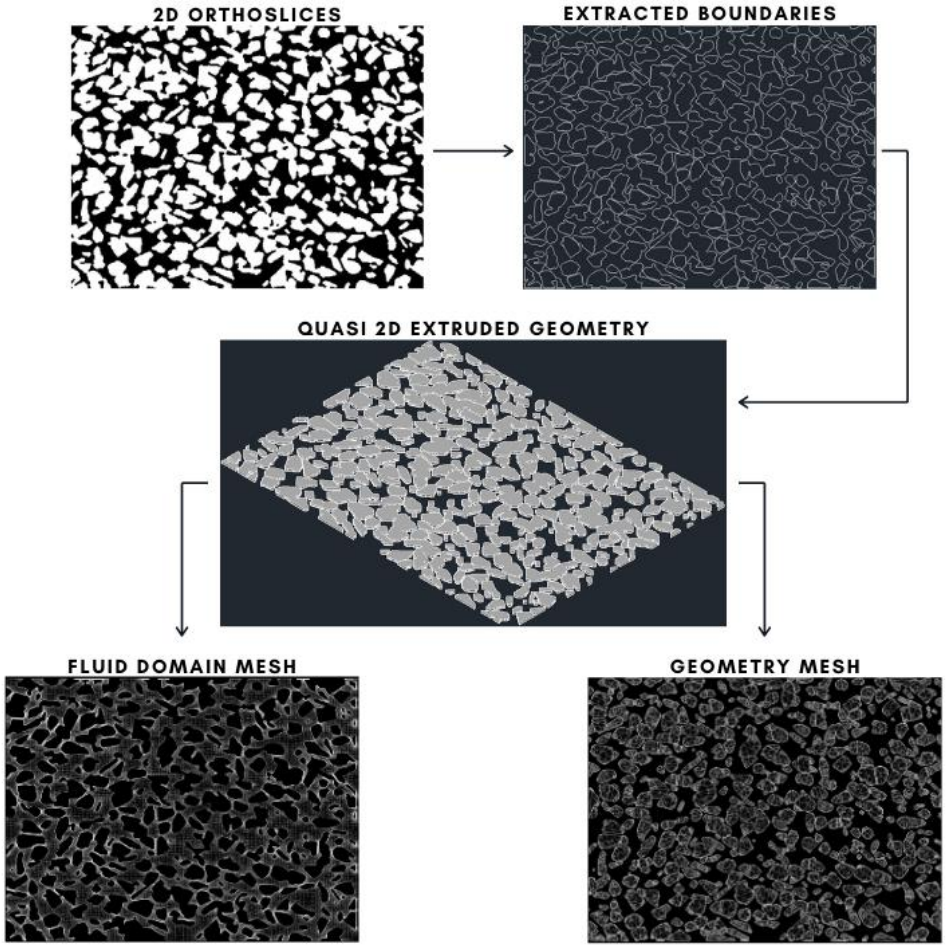

Figure 4: Geometry creation map from sample pore scale image to both DEM and CFD model meshes.

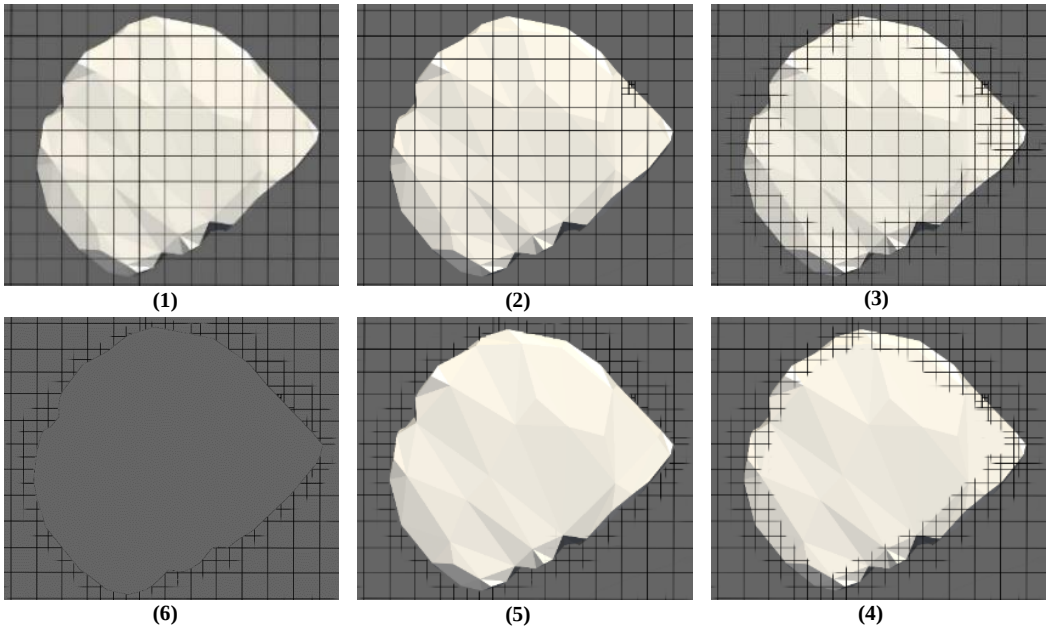

Figure 5 Steps to create the mesh for the fluid domain around the grain particles.

3.2. Mathematical Model

3.2.1. Fluid flow equations

The fluid flow model was calculated using the finite volume method, where the fluid domain is represented by small control volumes in which the mass and momentum of the fluid are calculated (Boudet 2011; Lomax et al. 2002). Determination of the field mass and momentum was done by integrating the governing equations over the domain cells. The CFD open-source toolbox OpenFOAM solves the coupled Navier-Stokes equations [Eq.1a] and the continuity equation [Eq.1b] for incompressible fluid to calculate the pressure p and velocity u (Weller et al. 1998).

$$\frac{\partial}{\partial t}(\rho u) + \nabla \cdot (\rho u u) = \nabla p + \left[\nabla \cdot \left(\mu(\nabla u + \nabla u^T)\right)\right] + F_{sa} \quad [1.a]$$

$$\nabla \cdot u = 0 \quad [1.b]$$

Where ρ is the fluid density, μ is the dynamic viscosity and F_{sa} is the net external force that could affect the fluid body. Figure 6 shows the boundary conditions for pressure and velocity. The flow was modeled as pressure-driven , hence pressure values at both the inlet and outlet are constant, while the velocity is calculated. The two sides

are considered as symmetrical, whereby the velocity condition is a slip-condition. On the other hand, the mesh boundary that represents the boundaries between the grain particles and the fluid domain has a no-slip velocity condition. This ensures that the velocity at the surface of the grain particles is zero.

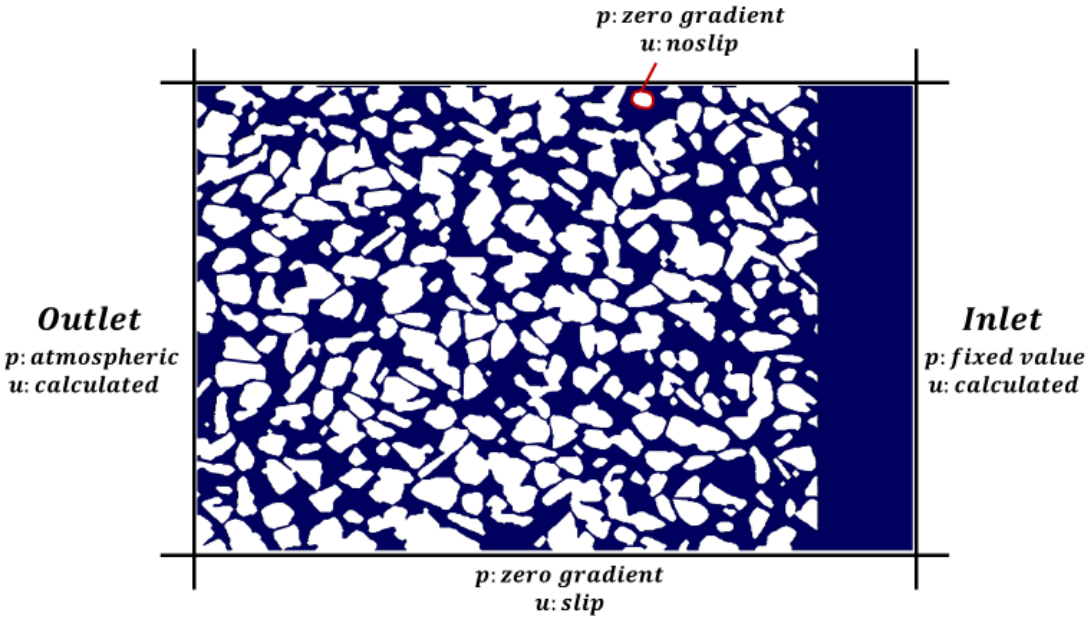

Figure 6 Pressure and velocity boundary conditions for the fluid domain.

3.2.2. Equations Governing particle interactions

Discrete Element Method (DEM) is a Lagrangian approach for calculating the trajectory of each particle in a large granular system (Kloss et al. 2012). The particle trajectory is calculated by considering the interactions between other particles/walls and how they influence the particles' behavior. Particle motion encompassed by translation and rotational changes. Newton's laws for translation and rotational motion are derived from the following equations for each particle i [Eq.2a&b].

$$m_i \frac{dv_i}{dt} = m_i g + \sum_{N_p} F_i^{p-p} + \sum_{N_w} F_i^{w-p} + F_i^{f-p} \quad [2.a]$$

$$I_i \frac{d\omega_i}{dt} = \sum_{N_p} r_{ic} \times F_i^{p-p} + \sum_{N_w} r_{ic} \times F_i^{w-p} + T_i^{f-p} \quad [2.b]$$

Where m_i is the particle mass, v_i is the velocity, g is the gravitational acceleration and N_p and N_w are the numbers of particles and walls, respectively. F_i^{p-p},

F_i^{w-p} and F_i^{f-p} are the forces applied from the other particles, wall, and fluid, respectively, on the particle i. For the torque equation, I_i is the particle inertia, ω_i is the angular velocity and r_{ic} is the torque radius. The calculation of the force acting on the particle i coming from another particle j is calculated based on the granular hertz model as in Figure.7 as two components normal and tangential (Ai et al. 2011; Brilliantov et al. 1996; Di Renzo and Di Maio 2005; Schwager and Pöschel 2007; Silbert et al. 2001; Zhang and Makse 2005). The normal force [Eq.3a] is calculated by two terms. One that represents the spring force, which depends on the normal overlap δn_{ij}. The other term is the damping force, which depends on the normal relative velocity vn_{ij}. The tangential force [Eq.3b] consists of two components as well. The shear force, which depends on the tangential overlap δt_{ij}. The other one is the damping force, which depends on the tangential relative velocity vt_{ij}.

$$F_n = k_n \delta n_{ij} - \gamma_n v n_{ij} \quad [3.a]$$

$$F_t = k_t \delta t_{ij} - \gamma_t v t_{ij} \quad [3.b]$$

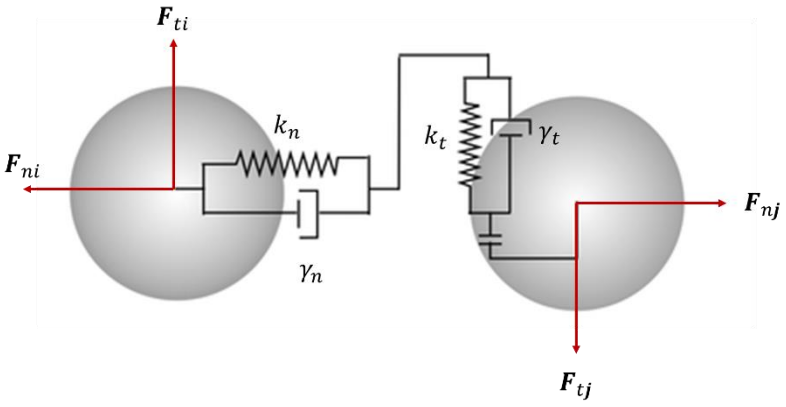

Figure 7: Granular model hertz illustration for particle interactions used in the DEM model.

For the time that the particles are in contact with the 'history' effect, the shear force induces the tangent displacement between the particles. k_n and k_t represent the elastic constants for normal and tangential contact, while γ_n and γ_t are the isoelastic

damping constant for normal and tangential contact respectively. The coefficients k and γ are calculated based on the material properties defined for the particles such as Young's and the shear modulus, Poisson ratio, and the coefficient of restitution. The same model is used to calculate the interactions between fine and grain particles.

3.2.3. Coupling scheme equations

The CFD-DEM coupling approach is a four-way coupling model, where fluid-particle interactions are included, as well as the particle-particle interactions. The coupling method is an Eulerian-Lagrangian method that accounts for the granular phase by introducing a volume fraction α_l into Navier-Stokes equations [Eq.4] (Goniva et al. 2012; Zhou et al. 2010).

$$\frac{\partial}{\partial t}(\alpha_l \rho_l u) + \nabla \cdot (\alpha_l \rho_l u u) = -\nabla p - K_{sl}(u - v) - F_{s-l} + \nabla \tau + \alpha_l \rho_l g \quad [4.a]$$

$$\nabla \cdot (\alpha_l u) = 0 \quad [4.b]$$

$$K_{sl} = \frac{\alpha_l |\sum F|}{\forall_{cell} |u - v|} \quad [4.c]$$

$$F_{s-l} = \frac{(F_{drag} + F_{Archim})}{\alpha_l} - \alpha_l \forall_l g \quad [4.d]$$

Where τ represents the viscous shear stress tensor and K_{sl} is the implicit momentum source term, $\forall_l$ and $\forall_{cell}$ are the fluid and the cell volumes. The drag force acting on each particle was calculated in a resolved manner using the method proposed by Shirgaonkar (Shirgaonkar, Maciver, and Patankar 2009). While the volumetric lift force was calculated from the density difference between fluid and particles. The coupled mathematical scheme is presented in the flow diagram below in Figure 8.

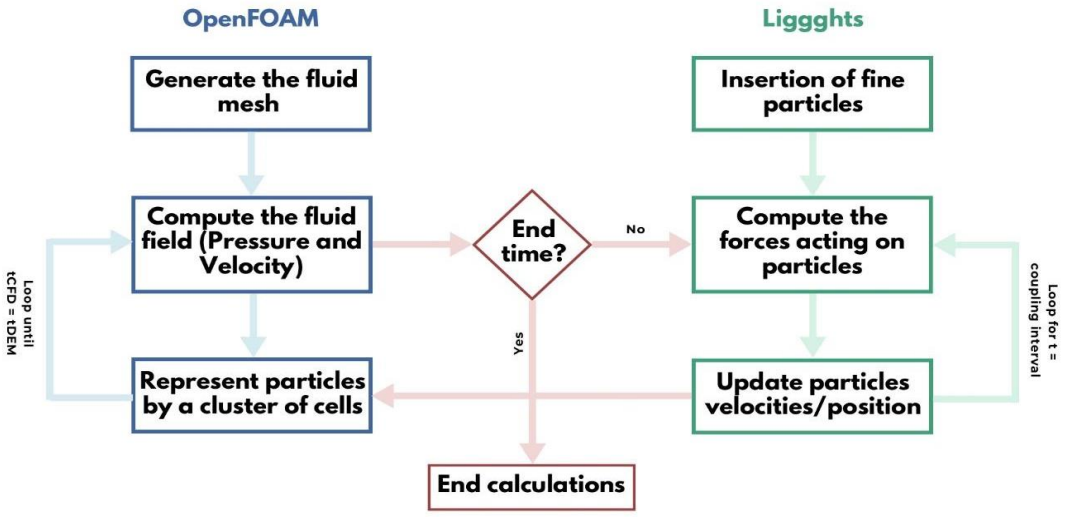

Figure 8 The CFD-DEM coupled model flow chart used to predict the fine migration behavior in porous media.

3.3. Numerical setup

3.3.1. Numerical solvers

First-time derivatives of parameters are calculated using the Euler discretization scheme, which uses the current time and previous time to evaluate the derivative as described in [Eq.5] for any parameter ϕ.

$$\frac{\partial}{\partial t}(\phi) = \frac{\phi - \phi_o}{\Delta t} \quad [5]$$

Linear interpolation is used to evaluate mesh face values, which is achieved by averaging the cell center values of cells on either side of the surface by assuming the parameter changes linearly between cell centers [Eq. 6]. One advantage of this scheme is that it is second-order accurate.

$$\phi_f = 0.5(\phi_c + \phi_d) \quad [6]$$

The divergence for the velocity and the viscous stress-tensor term in the fluid momentum equation is evaluated using the Gauss theorem with linear interpolation. The divergence for mass flux is also done using the Gauss theorem, but the Linear-Upwind Stabilized Transport interpolation scheme was used instead, as it is has shown

more stability. Additionally, for the calculation of the surface normal gradient, the scheme is uncorrected since the mesh is exclusively hexahedral (Agesen, Blæsbjerg, and Ehlers 2019). The Laplacian term of the fluid equation is solved using Gaussian integration with linear interpolation which is first-order accurate and bounded. Cell gradients are evaluated using the Gauss theorem which solves the volume integral as a surface integral [Eq. 7].

$$\int V(\nabla \cdot u)dV = \oint S(n \cdot u)dS \qquad [7]$$

The primary solver for the fluid flow is the Pressure Implicit with Splitting of Operators (PISO) algorithm**,** which is an extension of the Semi-Implicit Method for Pressure Linked Equations (SIMPLE) algorithm (Ferziger and Perić 2002; Issa 1986; Issa, Gosman, and Watkins 1986; Paulo J. Oliveira 2001). It operates based on a series of predictors and correctors until convergence. It starts by guessing the initial values for pressures and velocities and goes through a series of correctors to update the values. The algorithm repeats the steps of predicting and correcting until convergence to a certain tolerance of $T = 10^{-6}$. The one-dimensional momentum equation for the fluid, ignoring the gravity effect, [Eq. 8] is used to explain the PISO algorithm.

$$\frac{\partial u}{\partial t} + \frac{\partial}{\partial x}(uu) = \frac{\partial p}{\partial x} \qquad [8]$$

The predictor equation [Eq. 9a] discretizes the original equation using the schemes discussed before, where the predicted values are donated by $*$. The solution vector form [Eq. 9b] $\boldsymbol{C}$ is the coefficient array multiplying the solution $\boldsymbol{u}^*$vector and $\boldsymbol{r}$ is the right-hand side explicit source term without the pressure gradient. Then the matrix $\boldsymbol{C}$ is split into its diagonal matrix $\boldsymbol{A}$ and its off-diagonal matrix $\boldsymbol{H'}$ as shown in [Eq. 9c], the equation is solved for the predicted velocity value.

$$\left[\frac{1}{\Delta t} + \left(\frac{u^n_{i+\frac{1}{2}} - u^n_{i-\frac{1}{2}}}{2\Delta x}\right)\right] u^*_i + \left(\frac{u^n_{i+\frac{1}{2}}}{2\Delta x}\right) u^*_{i+1} - \left(\frac{u^n_{i-\frac{1}{2}}}{2\Delta x}\right) u^*_{i-1} = \frac{u^n_i}{\Delta t} - \left(\frac{\partial p}{\partial x}\right)\Big|^n_i \qquad [9.a]$$

$$Cu^* = r - \nabla p^n \quad [9.b]$$

$$Au^* + H'u^* = r - \nabla p^n \quad [9.c]$$

The discretized explicit velocity corrector equation [Eq. 10a] uses the predicted velocity and pressure values $\boldsymbol{u}^*, \boldsymbol{p}^*$as well as the old value of the velocity $\boldsymbol{u^n}$ to solve for the corrected velocity $\boldsymbol{u}^{**}$ as in [Eq. 10b]. The value of the velocity is calculated using the Preconditioned Bi-Conjugate Gradient (PBiCGStab) numerical solver, which has good parallel scaling (Barrett et al. 1994; van der Vorst 1992). While the pressure value is calculated using the Generalized Geometric-Algebraic Multi-Grid (GAMG) solver.

$$\left[\frac{1}{\Delta t} + \left(\frac{u^n_{i+\frac{1}{2}} - u^n_{i-\frac{1}{2}}}{2\Delta x}\right)\right] u_i^{**} + \left(\frac{u^n_{i+\frac{1}{2}}}{2\Delta x}\right) u^*_{i+1} - \left(\frac{u^n_{i-\frac{1}{2}}}{2\Delta x}\right) u^*_{i-1} = \frac{u_i^n}{\Delta t} - \left(\frac{\partial p}{\partial x}\right)\Big|_i^* \quad [10.a]$$

$$u^{**} = A^{-1}H - A^{-1}\nabla p^* \quad [10.b]$$

Where; $H = \boldsymbol{r} - \boldsymbol{A^{-1}H'}$ [10.c]

Geometric Agglomerated Algebraic Multigrid solver (GAMG) was used for the pressure as well as the volumetric flux. The GAMG solver works by creating a coarse grid using different agglomeration and coarsening algorithms. These agglomeration algorithms can either be geometric, using the mesh geometry, or algebraic, by applying the same techniques to the matrix itself. The coarse grid is then used to create an initial solution for the fine grid (Behrens 2009). The velocity and nuTilda are solved using Preconditioned Biconjugate Gradient Solver (Bi-CGSTAB) since it is a faster more smoothly converging variant of Bi-CG. It also uses a preconditioner to accelerate its convergence (van der Vorst 1992).

To consider the effect of flowing particles in the fluid domain, the Immersed Boundary Method (IBM) is used. Peskin (1972) was the first to introduce IBM to simulate cardiac mechanics and related blood flow (Peskin 1972). One of the

advantages of using an IBM is to facilitate grid generation, as the body does not have to conform to the cartesian grid explicitly. Another advantage is that the complexity of the domain geometry when simulating a non-boundary conforming Cartesian grid does not significantly affect the grid complexity and quality. Also, due to the stationary non-deforming Cartesian grid, IBM can deal with moving boundaries (Bandringa 2010; Tu, Yeoh, and Liu 2018). For simplicity, consider a rectangular field containing both the fluid region and the bond solid in Figure 9. When IBM is used to solve fluid flow within the complex geometry, the resulting rectangular domain would consist of fluid regions, in which the fluid velocity is governed by Navier-Stokes equations, and solid regions have a velocity of zero. The marker function $M(x)$ [Eq. 11] is then used to adjust the flow velocity results in the equation below [Eq. 12] (Tryggvason 2016).

$$M(x) = \begin{cases} 1 & in\ the\ fluid \\ 0 & in\ the\ solid \end{cases} \quad [11]$$

$$u(x) = M(x)\,u(x) + \big(1 - M(x)\big)\,v(x) \quad [12]$$

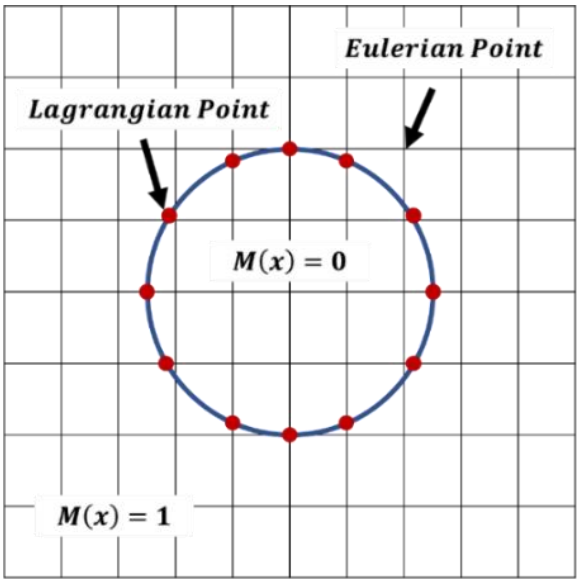

Figure 9: Immersed Boundary Method (IBM) illustration for particle covering fluid cells.

For each time step, a particle's associated properties (position, velocity, angular velocity, force, etc.) in the DEM solver are calculated by using the previous time step pressure field as well as velocity. Then, considering the solid phase in the mesh, the Navier-Stokes equations are solved in the complete fluid domain where each particle is represented by a cluster of cells. The fluid velocity is calculated in the CFD solver along with the pressure, depending on the precise position of the particles. Finally, the velocity and pressure fields correction of the fluid phase takes place using the particle's information. This process is repeated with every step up to the end of the simulation period (Goniva et al. 2011; Hager et al. 2014). The void fraction, which is used in the governing equations explained above, defines the space that particles occupy in a fluid cell. The void fraction field is placed in cells whose centers fall within the particle's body. One disadvantage of this model is that the particle should cover approximately eight cells to have accurate results. This was avoided by increasing the region in which the particles influence by scaling them up with a constant volume, for calculation of the void fraction (Goniva et al. 2012).

3.3.2. Time step choice

The stability of the CFD model depends heavily on the time step choice. A reliable method of determining the appropriate time step is the use of the Local Courant number, shown in [Eq. 13]

$$Co = \frac{|u_{cell}|\ \Delta t_{CFD}}{\Delta x} \qquad [13]$$

Where Co is Courant number and Δx is the cell length. The timestep is set so that the courant number value does not exceed one; to ensure that the fluid does not travel a distance greater than the cell length per time step (Agesen et al. 2019). For the DEM time step choice, Δt_{DEM} must be small enough to capture a collision between two or more particles. Hertz criteria [Eq.14] could be used to obtain a sufficient Δt_{DEM}.

$$\Delta t_{DEM} = 2.87 \left(\frac{m_{eff}^2}{r_{eff} E_{eff}^2 U_{max}} \right)^{\mathbf{0.2}} \quad [14]$$

Where m_{eff}, r_{eff} and E_{eff} are the particle's effective mass, radius, and Young's Modulus respectively. The time for DEM simulations is typically about 10^{-7} and could reach lower values in the case of stiff materials with a high Young's Modulus (Norouzi et al. 2016), however, by reducing Young's Modulus, the DEM time step could be increased (Agesen et al. 2019). The coupling interval is the number of DEM time steps that run before sending the particle data to the CFD solver. Thus, a coupling interval of ten means, that ten DEM iterations are calculated for each CFD iteration. The coupling interval CI is calculated as shown below [Eq. 15]. CI should be always an integer that is higher than or equal to one, where Δt_{CFD} is at most is equal to Δt_{DEM}.

$$CI = \frac{\Delta t_{DEM}}{\Delta t_{CFD}} \quad [15]$$

3.4. Model parallelization

CFD and DEM models were both parallelized to achieve faster computation. Information was passed between processors using Message Passing Interface (MPI), a standardized inter-process communication standard. The parameters of both particles approaching processor boundary and boundary mesh elements are passed between processors. Two different geometries were simulated multiple times using a different number of processors to find the optimal (computation-wise) number of threads. The geometries used were taken from different image samples, both had the dimensions of 6.7 mm by 5 mm and porosities of 0.503 in Figure10a and 0.421 in Figure.10b.

Throughout the simulations, the ideal number of processors for lowering the computational time was the physical processors (cores) and not the number of hyper-threads as shown in Figure.11. This could be due to the processes being CPU-bound as opposed to I/O bound.

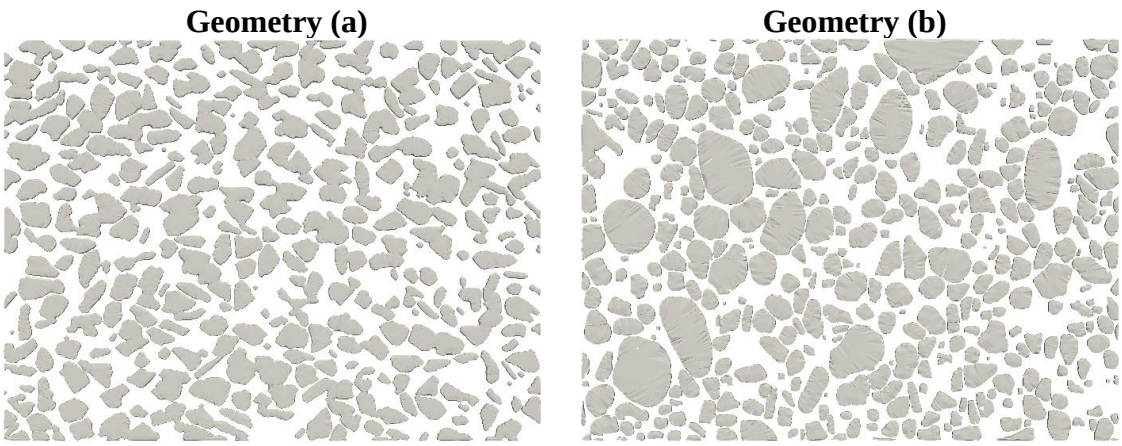

Figure 10: Pore-scale geometries used in the number of processors optimization for the parallelization step.

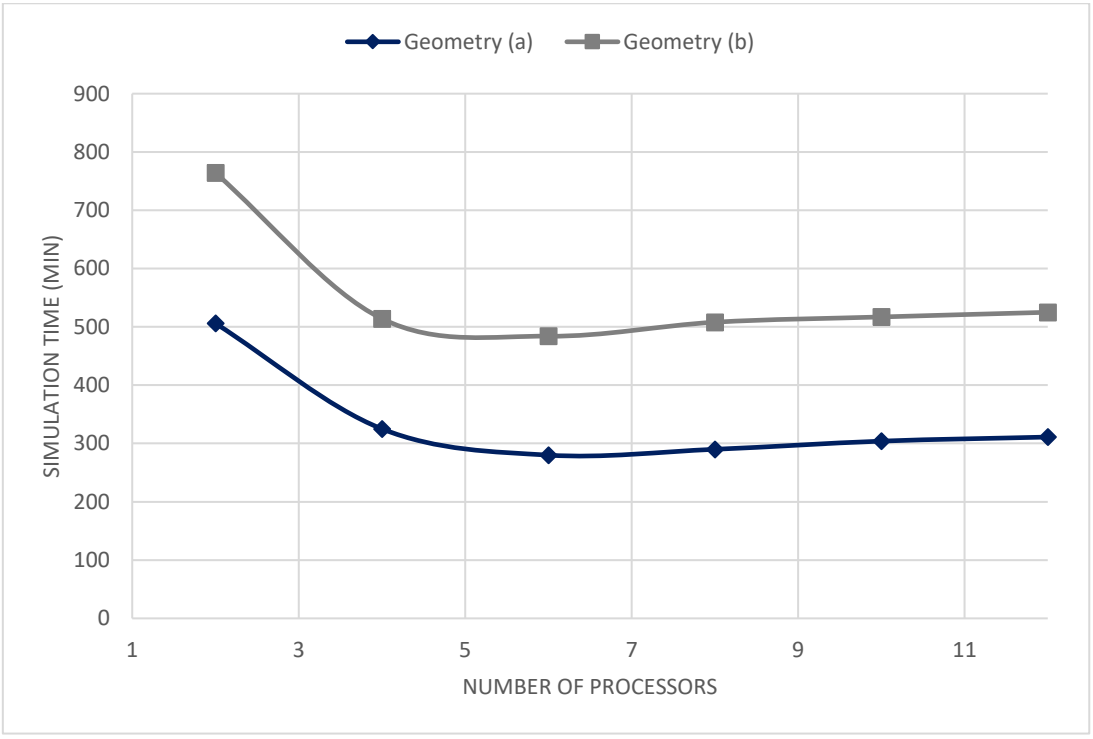

Figure 11: Simulation time for a different number of threads using a six-core machine.

CHAPTER 4: MICROMODEL EXPERIMENT

4.1. Description of the experiment

A micromodel experiment was performed to validate the coupled numerical model and verify that the model is capable of capturing the physical behavior. The experiment aimed to have pore visualization during the migration of fine particles in the reservoir rock. This was achieved using a two-dimensional microfluidic chip fabricated by Micronit Microfluidics BV by etching rock shaped structures on borosilicate glass to resemble the actual shape of rock as much as possible as shown in Figure 12c. The pore networks were etched on the glass plate and then fused with a plain glass wafer to form a quasi-two-dimensional porous network. The micromodel had a 20 μm depth and consisted of an etched area of 20 mm x 10 mm. The microfluidic channel surface had an average contact angle of 20^{o} which makes it hydrophilic. The micromodel permeability, porosity, and pore volume were 2.5 Darcy, 0.58, and 5.7μL respectively. The fine particles used in the experiment was modified carboxylate polystyrene latex particles (MAGSPHERE INC) with a diameter of 5 μm, with a density of 1.05 g/cm^3. Ten percent of the uniform polystyrene latex particles was diluted with water to prepare a 0.4% fines solution which was the optimal concentration for injection into the micromodel avoiding inlet pore plugging. The diluted suspension was agitated for 15 minutes before each experiment and was sonicated using an ultrasonic processor (SONICS, Vibra cell) in a water bath for 30 minutes in order to form a colloidal suspension. The experimental setup used in this study is schematically shown in Figure 12b (Nishad and Al-Raoush 2020). A microscope stage (Leica Z6 APO) was placed above the glass micromodel to view the behavior and interactions of the fine particles. A precision syringe pump (Kats Scientific, NE-1010) was connected to the inlet of the microchip to inject the colloidal solution, while the outlet was open to atmospheric

pressure. An area of 2.75 mm by 2 mm (Figure.12d) was captured and used to validate the numerical model presented in the previous section.

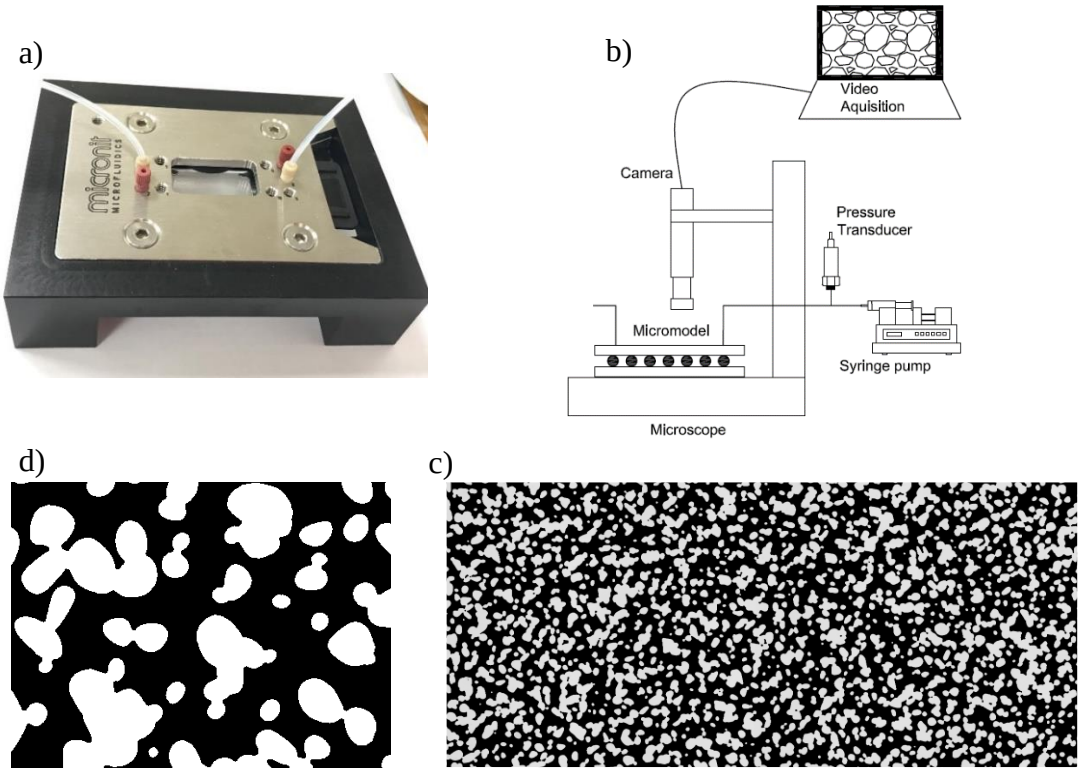

Figure 12: (a) The micromodel holder and chip. (b) Schematic of the experimental setup. (c) Full domain geometry and (d) the imaged field of view.

4.2. Experimental video analysis

The captured video was then divided into a set of consecutive images. These images were processed and manipulated using an open-source computer vision library OpenCV (Bradski 2000). Noise from the images was reduced through a combination of Gaussian blur (for the grayscale images) as well as dilation and erosion (for the binary image) techniques (Szeliski 2011). Grain particles were then isolated from each image and the fine particles were segmented using manual thresholding (Szeliski 2011). Contours describing the shape of each fine particle's perimeter were found using OpenCV's function findContours. This is done through linking the edges of each

isolated connected component i.e. each particle (Bradski 2000; Szeliski 2011). Those contours were subsequently used to calculate the coordinates of the center of each particle. The steps of the image processing workflow are presented in in Figure 13. Even though the microchip was cleaned thoroughly after each transport experiment, many particles remained attached to the bottom of the micromodel where the fluid flow was low (Nishad and Al-Raoush 2020). To ensure accurate measurements on the particles of interest, these attached particles must be disregarded prior to the measurements. This was accomplished by detecting the particles that have not moved throughout the entirety of the video.

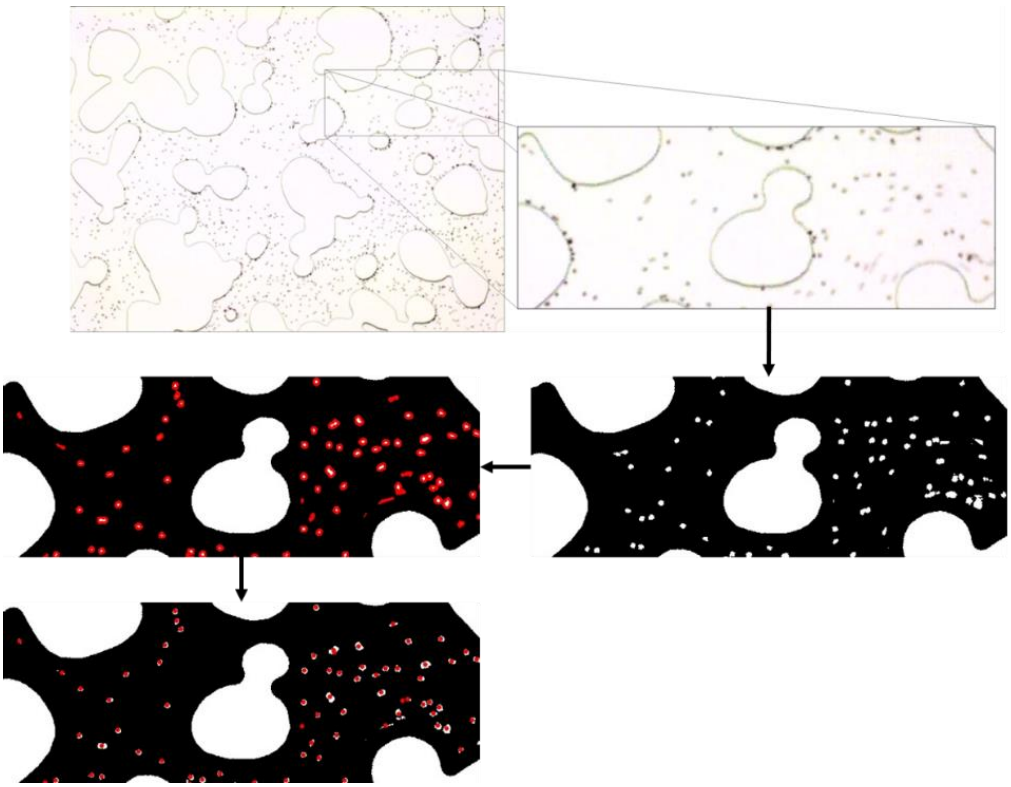

Figure 13: Images processing workflow using OpenCV.

Furthermore, the coordinates of each particle per image were used to approximate their velocities throughout the video by evaluating the displacement per image. For each particle, the next position is found by approximating candidate positions in the following frame to which the particle might have moved by using an

acceptance criterion. This criterion, as shown in Figure.14 below, is defined by setting a maximum displacement per frame as well as a minimum slope of displacement when the displacement is in the direction opposite of the flow of the fluid, both being approximated using an examination of the video as well as trial and error. The position that entails the lowest displacement is then chosen out of candidate positions as shown in Figure 14a below. By evaluating the displacement of each particle between frames, the velocity for each particle was calculated since the time between frames is known. A demonstration of these velocities in a particular image is shown below in Figure 14b where the length of the arrow represents the magnitude and the angle represents the direction.

a)

b)

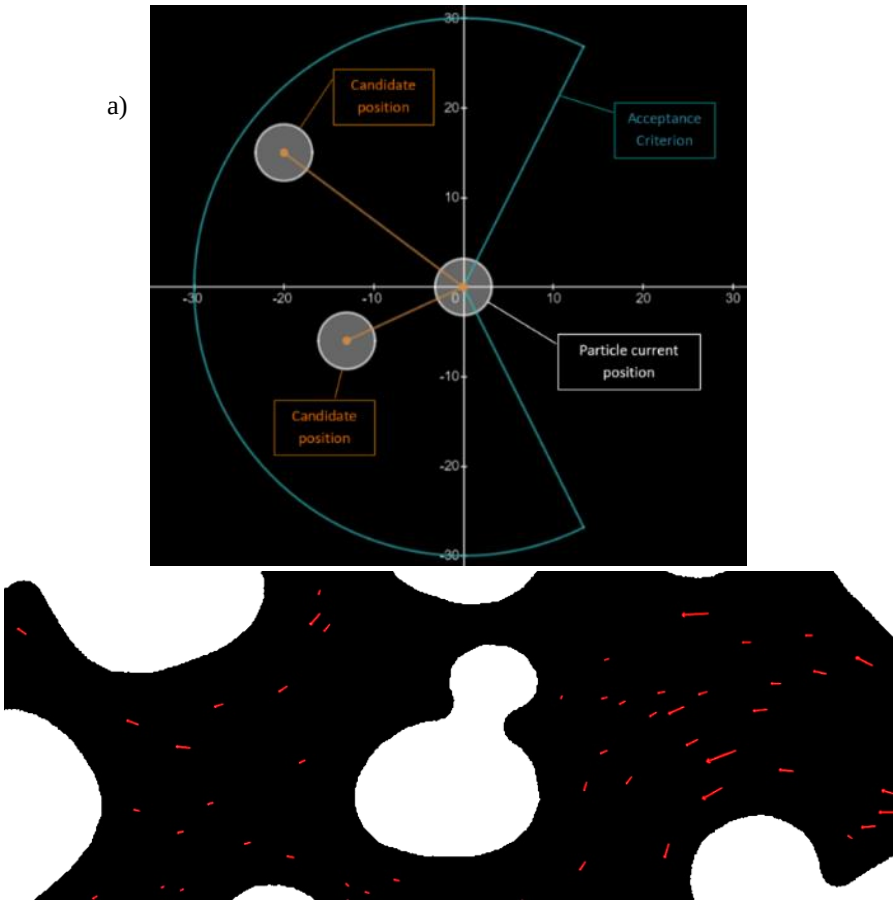

Figure 14 Criteria for determining the particle's position in consecutive frames.

CHAPTER 5: NUMERICAL MODEL VALIDATION

5.1. Fluid flow validation

In fluid mechanics, fluid movement around a basic geometry, such as a cylinder, is a traditional problem, with a significant number of experimental findings recorded in the literature. The fluid domain used for validation was $(50d \times 63d \times d)$ where $d = 0.1mm$, the cylinder was placed at $23d$ from the inlet face with a diameter of $2d$ as shown below in Figure.15. The model was validated by changing Reynold's number R_e [Eq. 16] and calculating the drag coefficient [Eq.17] from the model, and comparing it to the data presented in the literature.

$$R_e = \frac{u\,d}{\nu} \quad [16]$$

$$C_d = \frac{2\,F_{drag}}{\rho_f\,d\,u^2} \quad [17]$$

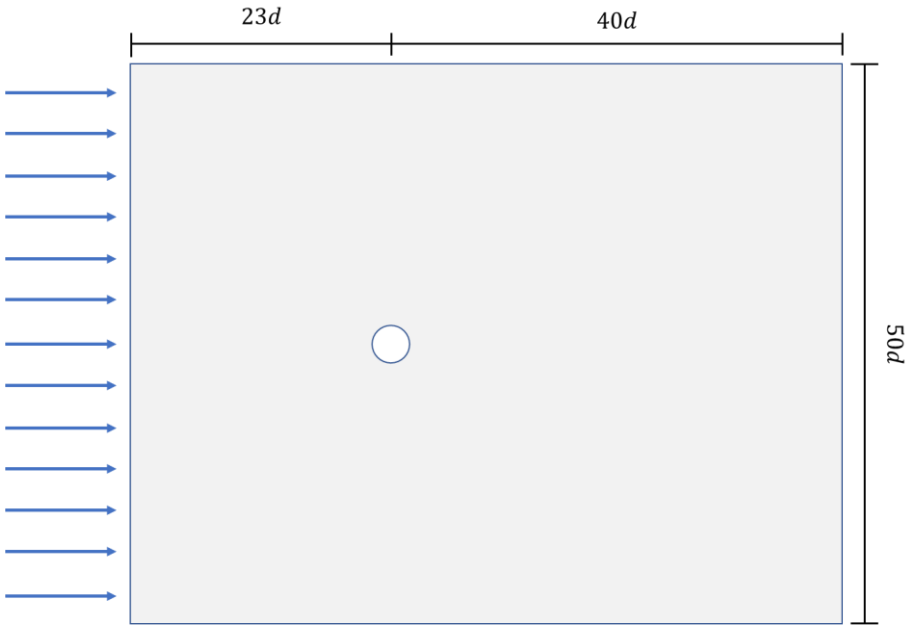

Figure 15: Flow around cylinder fluid domain for model validation.

Table.1 below shows the comparison between the mean drag coefficient for different Reynold's numbers for the proposed model and the results presented previously in the literature. There is good agreement between the results; hence, the

proposed model is deemed reliable for the flow prediction around simple geometries.

Table 1 Fluid flow validation of the model for simple geometry.

R_e	[1]	[2]	[3]	[4]	This Model
10	-	2.81	2.98	2.98	2.98
20	2.2	2.04	2.06	2.16	2.13
40	1.63	1.54	1.52	1.67	1.59
100	1.4	1.39	1.3	1.32	1.38

[1] (Su, Lai, and Lin 2007) [2] (Lima E Silva, Silveira-Neto, and Damasceno 2003)
[3] (Deng, Shao, and Ren 2006) [4] (Maniyeri 2014)

The microfluidic chip designed by Micronit was used to validate flow behavior for more complex geometries. The image was used to construct a model geometry (Figure 16) with the same physical dimensions to validate the fluid flow through porous media by comparing the permeabilities [Eq. 18], where k is the permeability.

$$k = \mu \frac{u\,L}{\nabla P} \qquad [18]$$

Table.2 below shows the porosity and permeability values obtained from the model and a comparison to the chip specifications from the manufacturer. It is clear from the results that the model is suitable for simulating the fluid flow in complex geometries. Moreover, the error between the results is not only based model deficiencies but could also related to inaccuracies in the geometric representation of the digitized and tessellated pore system. The etching technique used for the physical micromodel compared to the numerical model, along with enhancement done for the image during the image processing step created more path flows by eroding the grain particles, which could be noticed in the difference of porosities.

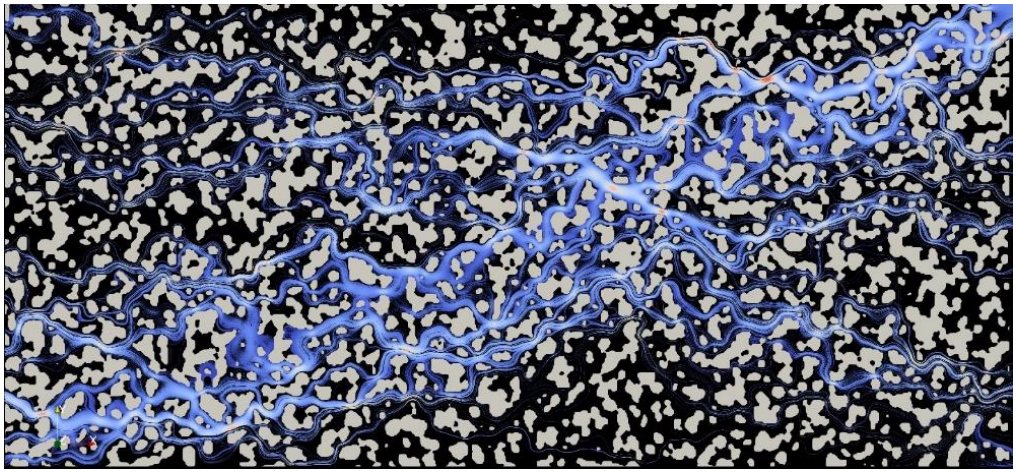

Figure 16: Flow in the microfluid chip domain for model validation.

Table 2: Microchip porosity and permeability results from the model compared to the manufacture specifications.

Parameters	Manufacture Spec.	Model Results
$Permeability\ (Darcy)$	2.5	2.65
$Porosity$	0.58	0.62

5.2. Coupled model validation

The validation of the full model is a significant phase in the modeling process. The goal is to confirm the ability of the proposed model to capture the physical behavior. After confirming the model's ability to capture the fluid flow behavior, the coupling of the fluid flow and particle interaction is compared to experimental results for fine migration in porous media. Using the data captured from both lab, as discussed in the micromodel experiment section, as well as the numerical model, the streamlines of both are compared as shown in Figure.17, which shows a significant anecdotal match between both. The micromodel streamlines were generated by fixing the chip geometry in the recorded video and fixing the particles positions from different frames into a single frame.

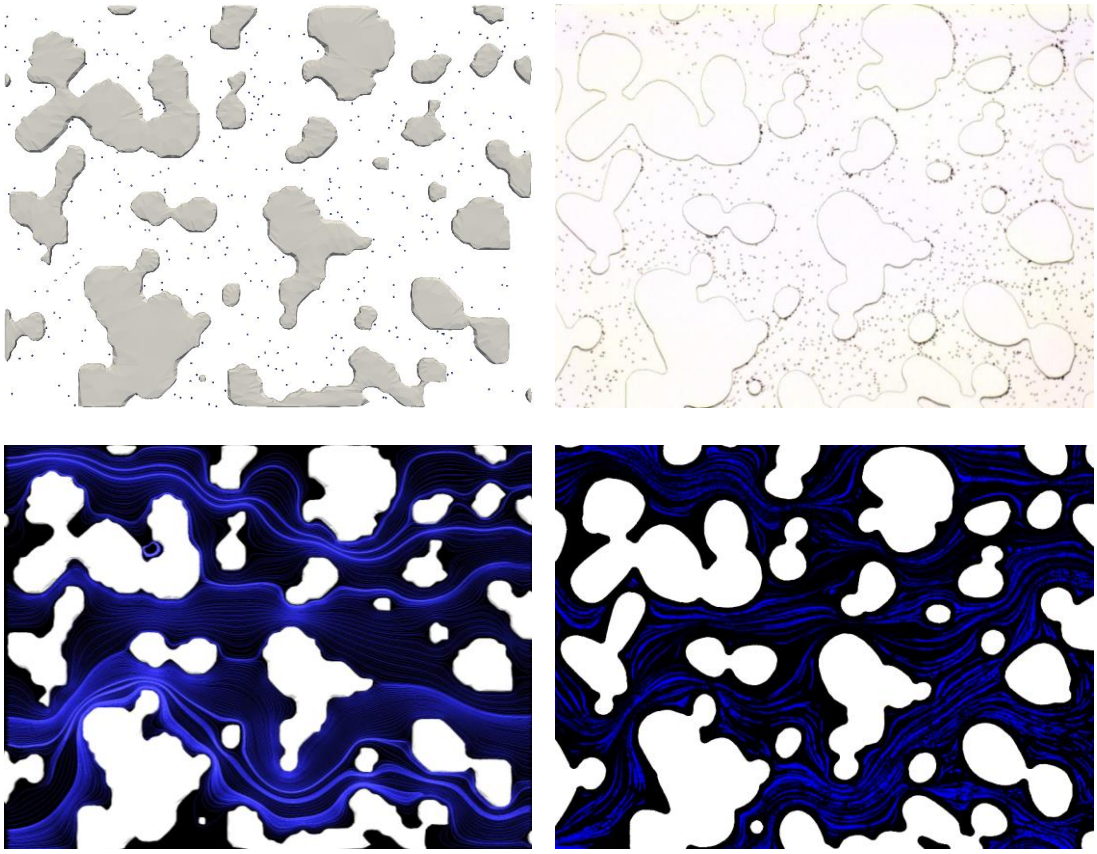

CFD-DEM Model **Lab Micomodel**

Figure 17: Comparison between flow streamlines produced by the numerical and physical micromodel.

After matching the initial experimental conditions, the average particle velocity trend over the course of the simulation and the micromodel were compared, in order to validate the coupled model. The graph below in Figure 18 shows both velocities, where a clear match in the velocity trends is observed.

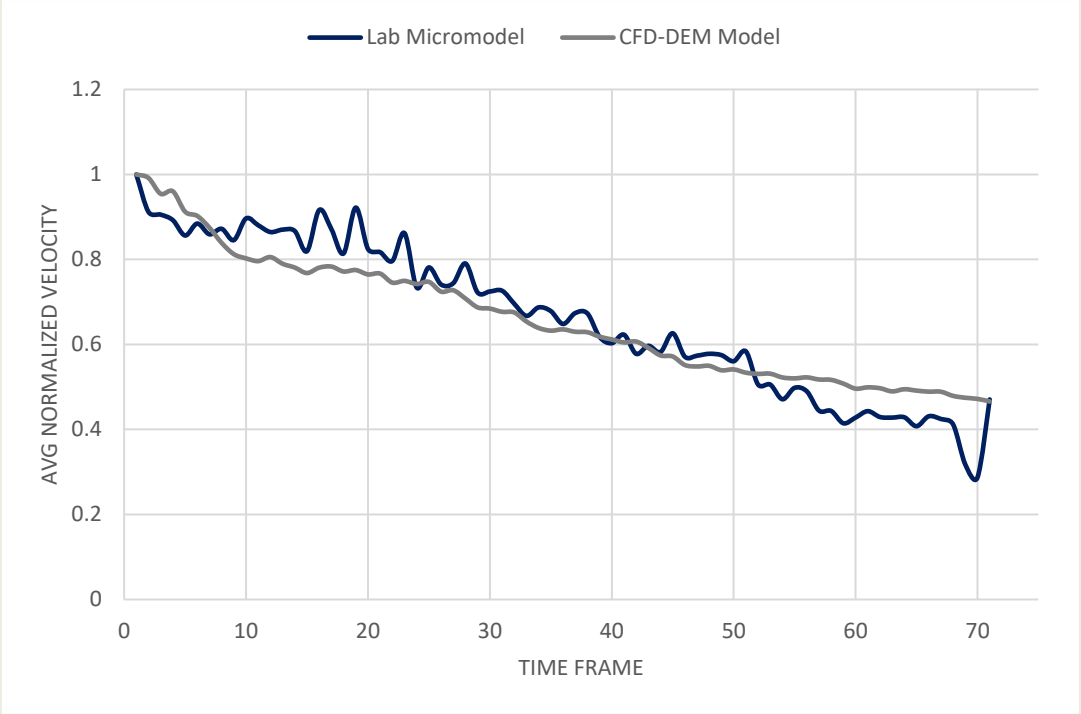

Figure 18: Average particle velocity trend comparison between the numerical and physical micromodel experiment.

The standard deviation of the particles' positions was used as an indication for the diffusion of the particles along with the simulation (Chin 2006). The standard deviation was calculated for the long dimension x as well as the smaller dimension y with time as presented in [Eq.19]. Where, x_i is the ith particle's position, μ is the mean position and N is the number of particles. The graphs below in Figure 19 show the standard deviation for the lab results against the model results, where the particles behavior showed good agreement and followed similar trends.

$$\sigma = \sqrt{\frac{\sum(x_i - \mu)^2}{N}} \qquad [19]$$

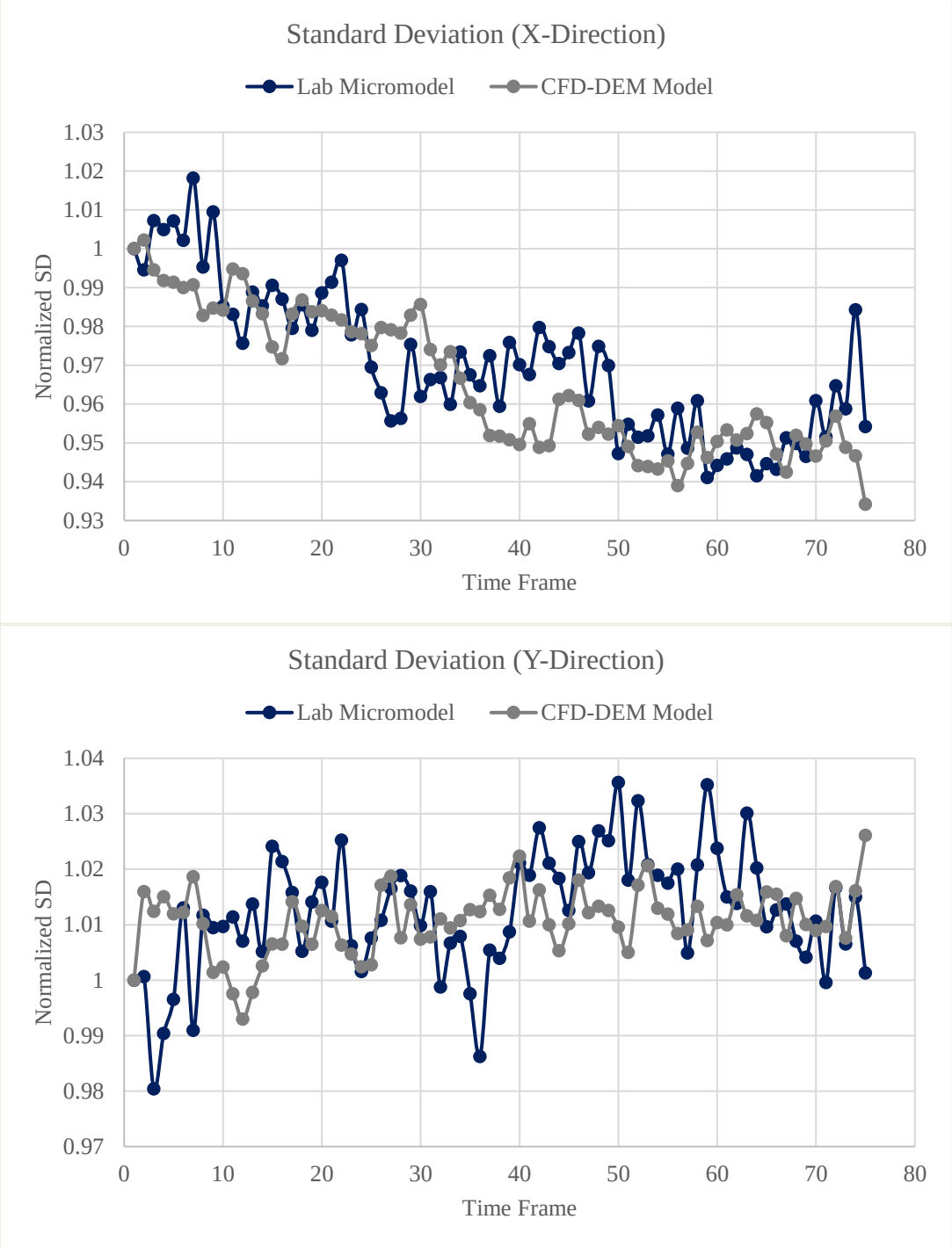

Figure 19: A comparison between the standard deviation of particle position for the numerical simulation and the micromodel.

CHAPTER 6: DISCUSSION AND CONCLUSIONS

6.1. Review

Fine particles transport in porous media has enjoyed considerable interest over the past few decades in various fields of science and engineering. On-site remediation strategies, enhanced transport of contaminants into aquifers, the permeability of gas and oil reservoirs, and artificial recharging of groundwater aquifers have become topics of concern. Fines migration has three primary impacts on the porous media system, which can facilitate contaminant transportation, decrease the system's chemical reactivity, and cause physical damage to the pore structure. As a result of the release and deposition of particles, the hydraulic characteristics of the pore medium may be modified, to the point of causing structural damage that may cause complete clogging of the porous media. There are two aspects of how fines migrate and cluster with respect to clogging of a pore-throat in single-phase flow. Mechanical processes through which particles block the throat due to the particle size or concentration. Chemical processes that cause fine particles, that are too small to clog pores, to cluster and become effective enough to block certain throat widths. The fate and transport of colloidal particles are generally affected by the parameters of the particles itself, the physical and chemical nature of the carrying fluid, and the grain particles parameters.

6.2. Numerical model setup

The model setup started with the geometry representation by acquiring the x-Ray Synchrotron Micro-Computed Tomography scans of different sand-pack samples as 3D images (Jarrar et al. 2018). Two-dimensional sections were taken from the original scans as segmented images that were converted to line drawings and then extruded and converted to mesh for the grain particle representation. The fluid domain mesh was created from the empty domain around the grain particles by using

SnappyHexMesh library in OpenFOAM. After generating the model geometry, the mathematical formulation of both the fluid behavior and the particles interactions was set. The fluid flow was predicted by solving Navier-Stokes equations along with the continuity equation in OpenFOAM. While the particle interactions were predicted by using the Lagrangian approach DEM, where the trajectory of each particle was calculated by considering Newton's laws for translation and rotational motion. The CFD-DEM coupling approach was a four-way coupling model where the interactions between the fluid and the particles are included as well as the particle-particle interactions.

The primary solver for the fluid flow was the PISO algorithm**,** which is an extension of the SIMPLE algorithm (Ferziger and Perić 2002; Issa 1986; Issa et al. 1986; Paulo J. Oliveira 2001). The value of the velocity was calculated using the PBiCGStab numerical solver, which has good parallel scaling (Barrett et al. 1994; van der Vorst 1992). While the pressure value is calculated using the GAMG solver. To consider the effect of flowing particles in the fluid domain, IBM was used (Peskin 1972). Using IBM as a coupling scheme has the advantage of facilitating the generation of the grid, as the body doesn't have to conform to the cartesian grid necessarily. Another advantage is that the complexity of the geometry when simulating a non-boundary conforming Cartesian grid does not significantly affect the grid complexity and quality. The time steps used for the CFD solver were determined by ensuring the Local Courant number is less than one to ensure the solution stability. The DEM time step was chosen by Hertz criteria to capture a collision between two or more particles (Agesen et al. 2019). The CFD and DEM models were both parallelized to achieve faster computation using MPI. Throughout the optimization simulations, the ideal number of processors, to reduce the computation time, was found to be the physical

processors in the used machine and not the number of hyper-threads.

6.3. Micromodel experimental setup

A micromodel experiment was conducted to validate the numerical model. The micromodel chip (Micronit Microfluidics BV) consisted of a 20mm x 10mm etched area and a 20μm depth. The fine particles used in the experiment were modified Carboxylate polystyrene latex particles (MAGSPHERE INC) with 5 μm diameter. The fine particles had a density of 1.05 g/cm^3, and it was injected into the microchip with a 10% concentration. A microscope stage (Leica Z6 APO) was placed above the glass micromodel to view the behavior and interactions of the fine particle. A precision syringe pump (Kats Scientific, NE-1010) was connected to the inlet of the microchip to inject water along with the fine particles while the outlet was open to atmospheric pressure. The experiment was recorded for a small area of 2.75mm x 2mm to be used in the numerical model validation.

6.4. Experimental video analysis

The video captured from the micromodel experiment was divided into a sequence of images. The images were processed and edited using the OpenCV python library (Bradski 2000). The noise has been removed from the images by combining Gaussian blur as well as methods for dilating and erosion (Szeliski 2011). The grain particles were removed from every image by using a simple thresholding technique (Szeliski 2011). The contours that define the form of each fine particle were found with the integrated findContours feature in OpenCV. Subsequently, these contours were used to predict the center coordinates of each particle. Besides, the coordinates of each particle per image were used to estimate the particles average velocity by measuring the displacement of each particle between every two frames. The challenge in estimating the velocity of the particles is to predict the right position of the particle in the next frame. This was solved by applying the success criteria for the candidate

positions and chose the highest probability position. By evaluating the displacement of each particle between frames, the velocity was calculated since the time between frames is known.

6.5. Numerical model validation

The numerical model was validated by validating the fluid flow first then the whole coupled model. The fluid flow was validated by comparing it to two geometries, the first geometry was the conventional flow around cylinder problem. The model was validated by changing Reynold's number R_e and calculate the drag coefficient from the model and compare it to the data presented in the literature. The model results showed very good agreement with the literature which validates the model's reliability for predicting the fluid flow around simple geometry. The second geometry for the flow validation was the microfluidic chip geometry used in the experiment. The microchip image was used to generate the numerical model geometry with the same physical dimensions. The flow was validated by comparing the microchip real permeability to the one calculated from the model. It was clear from the comparison that the numerical model is applicable for simulating the fluid flow in complex geometry.

After confirming the model's validity in predicting the fluid flow, the recorded video from the micromodel experiment was used to validate the coupled numerical model. The streamlines of both the CFD-DEM model as well as the micromodel were compared for the same geometry. The micromodel streamlines were generated by fixing the chip geometry in the recorded video and stabling the particles from different frames into a single frame. A significant match was clear between the two streamlines, where any insignificant deviation was because of the difference in the boundary conditions. After aligning the initial conditions of both models, the average particles velocity trends were compared as validation for the model. The average particles

velocity trend in the CFD-DEM model was smoother than the micromodel mainly because of the noise and imperfections in the recoded video. However, the velocity trends were in great agreement which validates the coupled numerical model. The standard deviation of the particles' positions was used as an indication for the diffusion of the particles along with the simulation (Chin 2006). The standard deviation was calculated for the long dimension x as well as the smaller dimension y with time. The standard deviation for the lab results against the model results showed that the behavior of the particles matched and followed very similar trends. This proved the CFD-DEM model's validity in predicting the fine particles' fate and transport in porous media within acceptable numerical errors.

6.6. Conclusions

1- The CFD-DEM model coupled using IBM presented here proved its capability for capturing the physical behavior of fine particle transport and deposition in porous media. However, the model needed to be parallelized to reduce computational cost.

2- The parallelization of the model could be optimized by using the physical number of processors, where splitting over the number of hyper-threads does not positively affect the simulation time but rather increases it. This could be due to the processes being CPU-bound as opposed to I/O bound.

3- The open-source library OpenCV used in Python showed great potential to be used for image and video processing for the results captured from micromodel experiments. Which could be used for coupled model validations as well as data analysis. Additionally, the simple algorithm established to track the fine particles proved its validity as a very simple method to calculate the particles velocity in the video result from the micromodel experiment.

4- The future enhancements of such a model could include using a more realistic full

three-dimensional geometry to draw some physical conclusions about the behavior. Furthermore, the electrostatic charges of the particles could be included to capture forces such as DLVO interactions.

REFERENCES

Agbangla, Gbedo Constant, Éric Climent, and Patrice Bacchin. 2012. “Experimental Investigation of Pore Clogging by Microparticles: Evidence for a Critical Flux Density of Particle Yielding Arches and Deposits.” *Separation and Purification Technology* 101:42–48.

Agesen, Andreas, Line Blæsbjerg, and Anders Ehlers. 2019. *Particle Accumulation in Square Duct Cavity with Laminar Flow*.

Ai, Jun, Jian-Fei Chen, J. Michael Rotter, and Jin Y. Ooi. 2011. “Assessment of Rolling Resistance Models in Discrete Element Simulations.” *Powder Technology* 206(3):269–82.

Argent, Joel, Saeed Torkzaban, Stephen Hubbard, Helen Le, Tahmineh Amirianshoja, and Manouchehr Haghighi. 2015. “Visualization of Micro-Particle Retention on a Heterogeneous Surface Using Micro-Models: Influence of Nanoscale Surface Roughness.” *Transport in Porous Media* 109(2):239–53.

Auset, Maria and Arturo A. Keller. 2004. “Pore-Scale Processes That Control Dispersion of Colloids in Saturated Porous Media.” *Water Resources Research* 40(3).

Auset, Maria and Arturo A. Keller. 2006. “Pore-Scale Visualization of Colloid Straining and Filtration in Saturated Porous Media Using Micromodels.” *Water Resources Research* 42(12):1–9.

Bandringa, Henry. 2010. *Immersed Boundary Methods*.

Barrett, R., M. Berry, T. F. Chan, J. Demmel, J. Donato, J. Dongarra, V. Eijkhout, R. Pozo, C. Romine, and H. Van der Vorst. 1994. *Templates for the Solution of Linear Systems: Building Blocks for Iterative Methods, 2nd Edition*. Philadelphia, PA: SIAM.

Bedrikovetsky, Pavel, Fernando D. Siqueira, Claudio A. Furtado, and Antonio Luiz S. Souza. 2011. “Modified Particle Detachment Model for Colloidal Transport in Porous Media.” *Transport in Porous Media* 86(2):353–83.

Behrens, Tim. 2009. “OpenFOAM’s Basic Solvers for Linear Systems of Equations.” *Report* 18.

Boccardo, Gianluca, Daniele L. Marchisio, and Rajandrea Sethi. 2014. “Microscale Simulation of Particle Deposition in Porous Media.” *Journal of Colloid and Interface Science* 417:227–37.

Boccardo, Gianluca, Tiziana Tosco, Asako Fujisaki, Francesca Messina, Amir Raoof, David R. Aguilera, Eleonora Crevacore, Daniele L. Marchisio, and Rajandrea Sethi. 2020. “Chapter 13 - A Review of Transport of Nanoparticles in Porous Media: From Pore- to Macroscale Using Computational Methods.” Pp. 351–81 in *Micro and Nano Technologies*, edited by B. Bonelli, F. S. Freyria, I. Rossetti, and R. B. T.-N. for the D. and R. of W. P. Sethi. Elsevier.

Boudet, Jérôme. 2011. “Finite Volume Methods.” *Computational Fluid Dynamics* (January):1–24.

Bradford, Scott A., Hyunjung N. Kim, Berat Z. Haznedaroglu, Saeed Torkzaban, and Sharon L. Walker. 2009. “Coupled Factors Influencing Concentration-Dependent Colloid Transport and Retention in Saturated Porous Media.” *Environmental Science and Technology* 43(18):6996–7002.

Bradski, G. 2000. “The OpenCV Library.” *Dr. Dobb’s Journal of Software Tools*.

Brilliantov, Nikolai V, Frank Spahn, Jan-Martin Hertzsch, and Thorsten Pöschel. 1996. “Model for Collisions in Granular Gases.” *Phys. Rev. E* 53(5):5382–92.

Cao, Shuang C., Junbong Jang, Jongwon Jung, William F. Waite, Timothy S. Collett, and Pushpendra Kumar. 2018. “2D Micromodel Study of Clogging Behavior of

Fine-Grained Particles Associated with Gas Hydrate Production in NGHP-02 Gas Hydrate Reservoir Sediments." *Marine and Petroleum Geology* (April).

Cejas, Cesare M., Fabrice Monti, Marine Truchet, Jean Pierre Burnouf, and Patrick Tabeling. 2017. "Particle Deposition Kinetics of Colloidal Suspensions in Microchannels at High Ionic Strength." *Langmuir* 33(26):6471–80.

Chen, Zhaohui, Yingchuan Li, Yiting Xie, and Xudong Wang. 2017. "In-Situ Particle Migration and Plugging Mechanism in Unconsolidated Sandstone and Sanding Management." *Chemistry and Technology of Fuels and Oils* 53(5):759–67.

Chequer, L. and P. Bedrikovetsky. 2019. "Suspension-Colloidal Flow Accompanied by Detachment of Oversaturated and Undersaturated Fines in Porous Media." *Chemical Engineering Science* 198:16–32.

Chin, David A. 2006. *Water-Quality Engineering in Natural Systems*.

Corapcioglu, M. Yavuz and Shiyan Jiang. 1993. "Colloid-facilitated Groundwater Contaminant Transport." *Water Resources Research* 29(7):2215–26.

Coronado, Manuel and Martín A. Díaz-Viera. 2017. "Modeling Fines Migration and Permeability Loss Caused by Low Salinity in Porous Media." *Journal of Petroleum Science and Engineering* 150(July 2016):355–65.

Datta, S. and S. Redner. 1998. "Gradient Clogging in Depth Filtration." *Phys Rev* E 58:R1203.

Deng, Jian, Xue-Ming Shao, and An-Lu Ren. 2006. "A New Modification of the Immersed-Boundary Method for Simulating Flows with Complex Moving Boundaries." *International Journal for Numerical Methods in Fluids* 52(11):1195–1213.

Dersoir, B., A. B. Schofield, M. Robert de Saint Vincent, and H. Tabuteau. 2019. "Dynamics of Pore Fouling by Colloidal Particles at the Particle Level." *Journal*

of Membrane Science 573(August 2018):411–24.

Dersoir, Benjamin, Matthieu Robert de Saint Vincent, Manouk Abkarian, and Hervé Tabuteau. 2015. "Clogging of a Single Pore by Colloidal Particles." *Microfluidics and Nanofluidics* 19(4):953–61.

Dressaire, Emilie and Alban Sauret. 2017. "Clogging of Microfluidic Systems." *Soft Matter* 13(1):37–48.

Ferziger, Joel H. and Milovan Perić. 2002. *Computational Methods for Fluid Dynamics*. Vol. 53. Springer, Berlin, Heidelberg.

Frimmel, Fritz H., Frank von der Kammer, and Hans-Curt Flemming. 2007. *Colloidal Transport in Porous Media*.

Gao, Dapeng, Yuewu Liu, Tianjiao Wang, and Daigang Wang. 2018. "Experimental Investigation of the Impact of Coal Fines Migration on Coal Corewater Flooding." *Sustainability (Switzerland)* 10(11):1–12.

Genovese, Damiano and Joris Sprakel. 2011. "Crystallization and Intermittent Dynamics in Constricted Microfluidic Flows of Dense Suspensions." *Soft Matter* 7(8):3889–96.

Goniva, A., C. Kloss, N. G. Deen, J. A. M. Kuipers, and S. Pirker. 2012. "Influence of Rolling Friction on Single Spout Fluidized Bed Simulation." *Particuology* 10(5):582–91.

Goniva, C., C. Kloss, A. Hager, Gijsbert Wierink, and S. Pirker. 2011. "A Multi-Purpose Open Source CFD-DEM Approach." in *The 8th Int. Conf. on CFD in the in the Oil & Gas, Metallurgical and Process Industries, Trondheim, Norway 21-23 June 2011*.

Gruesbeck, C. and R. E. Collins. 2007. "Entrainment and Deposition of Fine Particles in Porous Media." *Society of Petroleum Engineers Journal* 22(06):847–56.

Hager, A., C. Kloss, S. Pirker, and C. Goniva. 2014. “Parallel Resolved Open Source CFD-DEM: Method, Validation and Application.” *The Journal of Computational Multiphase Flows* 6(1):13–27.

Han, Gyeol, Tae Hyuk Kwon, Joo Yong Lee, and Jongwon Jung. 2019. “Fines Migration and Pore Clogging Induced by Single- and Two-Phase Fluid Flows in Porous Media: From the Perspectives of Particle Detachment and Particle-Level Forces.” *Geomechanics for Energy and the Environment* (xxxx):100131.

He, Bao nan, Jiang tao He, Fei Wang, Yu qian Lian, and Yue kun Zhao. 2018. “Migration, Clogging, and Carbon Source Release of Nano Emulsified Vegetable Oil in Porous Media, Evaluated by Column Experiments.” *Bioremediation Journal* 22(1–2):33–42.

Hirabayashi, Shinichiro, Toru Sato, Keisuke Mitsuhori, and Yoshitaka Yamamoto. 2012. “Microscopic Numerical Simulations of Suspension with Particle Accumulation in Porous Media.” *Powder Technology* 225:143–48.

Isa, Lucio, Rut Besseling, Alexander N. Morozov, and Wilson C. K. Poon. 2009. “Velocity Oscillations in Microfluidic Flows of Concentrated Colloidal Suspensions.” *Physical Review Letters* 102(5):1–4.

Issa, R. I. 1986. “Solution of the Implicitly Discretised Fluid Flow Equations by Operator-Splitting.” *Journal of Computational Physics* 62(1):40–65.

Issa, R. I., A. D. Gosman, and A. P. Watkins. 1986. “The Computation of Compressible and Incompressible Recirculating Flows by a Non-Iterative Implicit Scheme.” *Journal of Computational Physics* 62(1):66–82.

Jang, Junbong, Shuang C. Cao, Laura A. Stern, Jongwon Jung, and William F. Waite. 2018. “Impact of Pore Fluid Chemistry on Fine-Grained Sediment Fabric and Compressibility.” *Journal of Geophysical Research: Solid Earth* 0(m):5495–

5514.

Jarrar, Zaher A., Riyadh I. Al-Raoush, Jamal A. Hannun, Khalid A. Alshibli, and Jongwon Jung. 2018. “3D Synchrotron Computed Tomography Study on the Influence of Fines on Gas Driven Fractures in Sandy Sediments.” *Geomechanics for Energy and the Environment* (xxxx):1–10.

de Jonge, L. W., C. Kjaergaard, and P. Moldrup. 2010. “Colloids and Colloid-Facilitated Transport of Contaminants in Soils.” *Vadose Zone Journal* 3(2):321.

Jung, J. W., J. Jang, J. C. Santamarina, C. Tsouris, T. J. Phelps, and C. J. Rawn. 2012. “Gas Production from Hydrate-Bearing Sediments: The Role of Fine Particles.” *Energy and Fuels* 26(1):480–87.

Kanimozhi, B., Vivek Thamizhmani, Venkat Pranesh, S. Senthil, and T. Arun Selvakumar. 2019. “Kaolinite Fines Colloidal Flow in High Temperature Porous Carbonate Media during Saline Water Injection.” *Journal of Petroleum Science and Engineering* 175(January):775–84.

Kanti Sen, Tushar and Kartic C. Khilar. 2006. “Review on Subsurface Colloids and Colloid-Associated Contaminant Transport in Saturated Porous Media.” *Advances in Colloid and Interface Science* 119(2):71–96.

Kartic, C. Khilar and Fogler H. Scott. 1998. *Migrations of Fines in Porous Media*. Kluwer Academic Publishers.

Khan, Hasan J., Maryam S. Mirabolghasemi, Hongtao Yang, Maša Prodanović, David A. DiCarlo, and Matthew T. Balhoff. 2017. “Study of Formation Damage Caused by Retention of Bi-Dispersed Particles Using Combined Pore-Scale Simulations and Particle Flooding Experiments.” *Journal of Petroleum Science and Engineering* 158(February):293–308.

Kheirabadi, Mohsen, Mohammad Hossein Niksokhan, and Babak Omidvar. 2017.

"Colloid-Associated Groundwater Contaminant Transport in Homogeneous Saturated Porous Media: Mathematical and Numerical Modeling." *Environmental Modeling and Assessment* 22(1):79–90.

Khilar, Kartic C. and H. Scott Fogler. 1983. "Water Sensitivity of Sandstones." *Society of Petroleum Engineers Journal* 23(01):55–64.

Kim, Ijung, Tongren Zhu, Sungmin Youn, and Desmond F. Lawler. 2017. "Polymer-Capped Nanoparticle Transport in Granular Media Filtration: Deviation from the Colloidal Filtration Model." *Journal of Environmental Engineering* 143(7):03117003.

Kloss, Christoph, Christoph Goniva, Alice Hager, Stefan Amberger, and Stefan Pirker. 2012. "Models, Algorithms and Validation for Opensource DEM and CFD-DEM." *Progress in Computational Fluid Dynamics* 12(2–3):140–52.

Lei, Haiyan, Likun Dong, Chuanxia Ruan, and Liya Ren. 2017. "Study of Migration and Deposition of Micro Particles in Porous Media by Lattice-Boltzmann Method." Pp. 4004–9 in *Energy Procedia*. Vol. 142. Elsevier B.V.

Li, Bowen, Chunpeng Zhang, Yan Li, Chunyu Wen, Jun Dong, Meng Yao, and Liming Ren. 2018. "One-Dimensional Experimental Investigation and Simulation on the Transport Characteristics of Heterogeneous Colloidal Mg(OH) 2 in Saturated Porous Media." *Journal of Contaminant Hydrology* 218(September):34–43.

Li, Qingjian and Valentina Prigiobbe. 2018. "Numerical Simulations of the Migration of Fine Particles Through Porous Media." *Transport in Porous Media* 122(3):745–59.

Li, Wanyi, Xueling Liu, and Xin Jiang. 2017. "Review on the Study on Migration and Deposition of Particles in Porous Media." *Transactions - Geothermal Resources Council* 41:1680–88.

Li, Zhelong, Dongxiao Zhang, and Xiqing Li. 2010. “Tracking Colloid Transport in Porous Media Using Discrete Flow Fields and Sensitivity of Simulated Colloid Deposition to Space Discretization.” *Environmental Science and Technology* 44(4):1274–80.

Lima E Silva, A. L. Fernande., Aristeus Silveira-Neto, and J. J. R. Damasceno. 2003. “Numerical Simulation of Two-Dimensional Flows over a Circular Cylinder Using the Immersed Boundary Method.” *Journal of Computational Physics* 189(2):351–70.

Liu, Dan, Jingjing Zhou, Wenjing Zhang, Ying Huan, Xipeng Yu, Fulin Li, and Xuequn Chen. 2016. “Column Experiments to Investigate Transport of Colloidal Humic Acid through Porous Media during Managed Aquifer RechargeExpériences En Colonne Pour Analyser Le Transport de l’acide Humique Colloïdale En Milieu Poreux Au Cours de La Recharge Artificielle d.” *Hydrogeology Journal* 25(1):79–89.

Liu, Qiang, Volha Lazouskaya, Qingxiang He, and Yan Jin. 2010. “Effect of Particle Shape on Colloid Retention and Release in Saturated Porous Media.” *Journal of Environment Quality* 39(2):500.

Lomax, H., TH Pulliam, DW Zingg, and TA Kowalewski. 2002. “Fundamentals of Computational Fluid Dynamics.” *Applied Mechanics Reviews*.

Maniyeri, Ranjith. 2014. “Numerical Study of Flow Over a Cylinder Using an Immersed Boundary Finite Volume Method.” *International Journal of Engineering Research* 3(4):213–16.

Massenburg, Sorell S., Esther Amstad, and David A. Weitz. 2016. “Clogging in Parallelized Tapered Microfluidic Channels.” *Microfluidics and Nanofluidics* 20(6):1–5.

McBride, M. B. and P. Baveye. 2010. “Diffuse Double-Layer Models, Long-Range Forces, and Ordering in Clay Colloids.” *Soil Science Society of America Journal* 66(4):1207.

Moghadasi, J., H. Müller-Steinhagen, M. Jamialahmadi, and A. Sharif. 2004. “Theoretical and Experimental Study of Particle Movement and Deposition in Porous Media during Water Injection.” *Journal of Petroleum Science and Engineering* 43(3–4):163–81.

Mojid, M. A. and H. Cho. 2006. “Estimating the Fully Developed Diffuse Double Layer Thickness from the Bulk Electrical Conductivity in Clay.” *Applied Clay Science* 33(3–4):278–86.

Molnar, Ian L., William P. Johnson, Jason I. Gerhard, Clinton S. Willson, and Denis M. O’Carroll. 2015. “Predicting Colloid Transport through Saturated Porous Media: A Critical Review.” *Water Resources Research*.

Muecke, T. W. 1979. “Formation Fines and Factors Controlling Their Movement in Porous Media.” *Journal of Petroleum Technology* 31(02):144–50.

Mustin, Benjamin and Boris Stoeber. 2010. “Deposition of Particles from Polydisperse Suspensions in Microfluidic Systems.” *Microfluidics and Nanofluidics* 9(4–5):905–13.

Nguyen, Cong Doan, Nadia Benahmed, Pierre Philippe, and Elizabeth Victoria Diaz Gonzalez. 2017. “Experimental Study of Erosion by Suffusion at the Micro-Macro Scale.” *EPJ Web of Conferences* 140:09024.

Nishad, Safna and Riyadh I. Al-Raoush. 2020. “Impact of Ionic Strength on Colloid Retention in a Porous Media: A Micromodel Study.” (Cic):715–23.

Norouzi, Hamid, Reza Zarghami, Rahmat Sotudeh-Gharebagh, and Navid Mostoufi. 2016. “DEM Formulation.” Pp. 15–67 in *Coupled CFD-DEM Modeling*. John

Wiley & Sons, Ltd.

Pandya, Vishal B., S. Bhuniya, and Kartic C. Khilar. 1998. “Existence of a Critical Particle Concentration in Plugging of a Packed Bed.” *AIChE Journal* 44(4):978–81.

Paulo J. Oliveira, Raad I. Issa. 2001. “AN IMPROVED PISO ALGORITHM FOR THE COMPUTATION OF BUOYANCY-DRIVEN FLOWS.” *Numerical Heat Transfer, Part B: Fundamentals* 40(6):473–93.

Peskin, Charles S. 1972. “Flow Patterns around Heart Valves: A Numerical Method.” *Journal of Computational Physics* 10(2):252–71.

Di Renzo, Alberto and Francesco Paolo Di Maio. 2005. “An Improved Integral Non-Linear Model for the Contact of Particles in Distinct Element Simulations.” *Chemical Engineering Science* 60(5):1303–12.

Richards, Kevin S. and Krishna R. Reddy. 2007. “Critical Appraisal of Piping Phenomena in Earth Dams.” *Bulletin of Engineering Geology and the Environment* 66(4):381–402.

Robert De Saint Vincent, Matthieu, Manouk Abkarian, and Hervé Tabuteau. 2016. “Dynamics of Colloid Accumulation under Flow over Porous Obstacles.” *Soft Matter* 12(4):1041–50.

Rodgers, M., J. Mulqueen, and M. G. Healy. 2010. “Surface Clogging in an Intermittent Stratified Sand Filter.” *Soil Science Society of America Journal* 68(6):1827.

Russell, Thomas, Duy Pham, Mahdi Tavakkoli Neishaboor, Alexander Badalyan, Aron Behr, Luis Genolet, Patrick Kowollik, Abbas Zeinijahromi, and Pavel Bedrikovetsky. 2017. “Effects of Kaolinite in Rocks on Fines Migration.” *Journal of Natural Gas Science and Engineering* 45:243–55.

Russell, Thomas, Kiet Wong, Abbas Zeinijahromi, and Pavel Bedrikovetsky. 2018.

"Effects of Delayed Particle Detachment on Injectivity Decline Due to Fines Migration." *Journal of Hydrology* 564:1099–1109.

Sadri, Behnam, David Pernitsky, and Mohtada Sadrzadeh. 2017. "Aggregation and Deposition of Colloidal Particles: Effect of Surface Properties of Collector Beads." *Colloids and Surfaces A: Physicochemical and Engineering Aspects* 530(July):46–52.

Saha, Amal Krishna, Alok Sinha, and Srinivas Pasupuleti. 2019. "Modification, Characterization and Investigations of Key Factors Controlling the Transport of Modified Nano Zero-Valent Iron (NZVI) in Porous Media." *Environmental Technology (United Kingdom)* 40(12):1543–56.

Salerno, Michael B., Matt Flamm, Bruce E. Logan, and Darrell Velegol. 2006. "Transport of Rodlike Colloids through Packed Beds." *Environmental Science and Technology* 40(20):6336–40.

Sanematsu, Paula C., Karsten E. Thompson, and Clinton S. Willson. 2019. "Pore-Scale Modeling of Nanoparticle Transport and Retention in Real Porous Materials." *Computers and Geosciences* 127(August 2018):65–74.

Santos, A. and P. Bedrikovetsky. 2006. "A Stochastic Model for Particulate Suspension Flow in Porous Media." *Transport in Porous Media* 62(1):23–53.

Sauret, Alban, Erin C. Barney, Adeline Perro, Emmanuel Villermaux, Howard A. Stone, and Emilie Dressaire. 2014. "Clogging by Sieving in Microchannels: Application to the Detection of Contaminants in Colloidal Suspensions." *Applied Physics Letters* 105(7).

Schwager, Thomas and Thorsten Pöschel. 2007. "Coefficient of Restitution and Linear–Dashpot Model Revisited." *Granular Matter* 9(6):465–69.

Sendekie, Zenamarkos B. and Patrice Bacchin. 2016. "Colloidal Jamming Dynamics in

Microchannel Bottlenecks." *Langmuir* 32(6):1478–88.

Sharma, Prabhakar, Hesham M. Abdou, and Markus Flury. 2008. "Effect of the Lower Boundary Condition and Flotation on Colloid Mobilization in Unsaturated Sandy Sediments." *Vadose Zone Journal* 7(3):930.

Shedid, Shedid A. and Mohamed A. Saad. 2017. "Comparison and Sensitivity Analysis of Water Saturation Models in Shaly Sandstone Reservoirs Using Well Logging Data." *Journal of Petroleum Science and Engineering* 156:536–45.

Shen, Chongyang, Yuanfang Huang, Baoguo Li, and Yan Jin. 2010. "Predicting Attachment Efficiency of Colloid Deposition under Unfavorable Attachment Conditions." *Water Resources Research*.

Sherard, James L., Lorn P. Dunnigan, and James R. Talbot. 2002. "Basic Properties of Sand and Gravel Filters." Pp. 1941–57 in *Geotechnical Special Publication*. Vol. 110.

Shirgaonkar, Anup A., Malcolm A. Maciver, and Neelesh A. Patankar. 2009. "A New Mathematical Formulation and Fast Algorithm for Fully Resolved Simulation of Self-Propulsion." *Journal of Computational Physics* 228(7):2366–90.

Silbert, Leonardo E., Deniz Erta\ifmmode \mbox\cs\else \cs\fi, Gary S. Grest, Thomas C. Halsey, Dov Levine, and Steven J. Plimpton. 2001. "Granular Flow down an Inclined Plane: Bagnold Scaling and Rheology." *Phys. Rev. E* 64(5):51302.

Sogami, Ikuo and Norio Ise. 1984. "On the Electrostatic Interaction in Macroionic Solutions." *The Journal of Chemical Physics* 81(12):6320–32.

Su, Junwei, Guoliang Chai, Le Wang, Weidong Cao, Zhaolin Gu, Chungang Chen, and Xiao Yun Xu. 2019. "Pore-Scale Direct Numerical Simulation of Particle Transport in Porous Media." *Chemical Engineering Science* 74(February):613–27.

Su, Shen-Wei, Ming-Chih Lai, and Chao-An Lin. 2007. “An Immersed Boundary Technique for Simulating Complex Flows with Rigid Boundary.” *Computers & Fluids* 36(2):313–24.

Szeliski, Richard. 2011. “Computer Vision Algorithms and Applications.”

Tan, Bo, Shuguang Liu, Chaomeng Dai, Hui Zhou, Zhenquan Hui, Guihui Zhong, and Hong Zhang. 2017. “Modelling of Colloidal Particle and Heavy Metal Transfer Behaviours during Seawater Intrusion and Refreshing Processes.” *Hydrological Processes* 31(22):3920–31.

Torkzaban, Saeed, Scott A. Bradford, and Sharon L. Walker. 2007. “Resolving the Coupled Effects of Hydrodynamics and DLVO Forces on Colloid Attachment in Porous Media.” *Langmuir*.

Tryggvason, Grétar. 2016. “Chapter 6 - Computational Fluid Dynamics.” Pp. 227–91 in *Fluid Mechanics (Sixth Edition)*, edited by P. K. Kundu, I. M. Cohen, and D. R. Dowling. Boston: Academic Press.

Tu, Jiyuan, Guan-Heng Yeoh, and Chaoqun Liu. 2018. “Chapter 9 - Some Advanced Topics in CFD.” Pp. 369–417 in *Computational Fluid Dynamics (Third Edition)*, edited by J. Tu, G.-H. Yeoh, and C. Liu. Butterworth-Heinemann.

Uchida, Shun, Jeen-shang Lin, Evgeniy M. Myshakin, Yongkoo Seol, Timothy S. Collett, and Ray Boswell. 2017. “Numerical Simulations of Sand Production in Interbedded Hydrate-Bearing Sediments during Depressurization.” *The 9th International Conference on Gas Hydrates*.

Unni, H. N. and C. Yang. 2008. “Kinetics of Colloidal Particle Deposition to a Solid Surface from Pressure Driven Microchannel Flows.” *The Canadian Journal of Chemical Engineering* 85(5):609–16.

Vaidya, R. N. and H. S. Fogler. 1990. “Formation Damage Due to Colloidally Induced

Fines Migration." *Colloids and Surfaces* 50(C):215–29.

van der Vorst, H. A. 1992. "Bi-CGSTAB: A Fast and Smoothly Converging Variant of Bi-CG for the Solution of Nonsymmetric Linear Systems." *SIAM Journal on Scientific and Statistical Computing*.

Waite, W. F., J. Jang, T. S. Collett, P. Kumar, Lars W. Chatrou, M. Pilar Escribano, Maria A. Viruel, Jan W. Maas, E. James, and José I. Hormaza. 2018. "Downhole Physical Property-Based Description of a Gas Hydrate Petroleum System in NGHP-02 Area C_ A Channel, Levee, Fan Complex in the Krishna-Godavari Basin Offshore Eastern India." *Marine and Petroleum Geology*.

Weller, H. G., G. Tabor, H. Jasak, and C. Fureby. 1998. "A Tensorial Approach to Computational Continuum Mechanics Using Object-Oriented Techniques." *Computers in Physics* 12(6):620–31.

Won, Jongmuk, Dongseop Lee, Khanh Pham, Hyobum Lee, and Hangseok Choi. 2019. "Impact of Particle Size Distribution of Colloidal Particles on Contaminant Transport in Porous Media." *Applied Sciences* 9(5):932.

Wyss, Hans M., Daniel L. Blair, Jeffrey F. Morris, Howard A. Stone, and David A. Weitz. 2006. "Mechanism for Clogging of Microchannels." *Physical Review E - Statistical, Nonlinear, and Soft Matter Physics* 74(6):1–4.

Yang, Y. and P. Bedrikovetsky. 2017. "Exact Solutions for Nonlinear High Retention-Concentration Fines Migration." *Transport in Porous Media* 119(2):351–72.

You, Zhenjiang, Yulong Yang, Alexander Badalyan, Pavel Bedrikovetsky, and Martin Hand. 2016. "Mathematical Modelling of Fines Migration in Geothermal Reservoirs." *Geothermics*.

Yu, M., F. Hussain, J. Y. Arns, P. Bedrikovetsky, L. Genolet, A. Behr, P. Kowollik, and C. H. Arns. 2018. "Imaging Analysis of Fines Migration during Water Flow

with Salinity Alteration." *Advances in Water Resources* 121(August):150–61.

Yuan, Hao and Alexander A. Shapiro. 2011. "A Mathematical Model for Non-Monotonic Deposition Profiles in Deep Bed Filtration Systems." *Chemical Engineering Journal* 166(1):105–15.

Zhang, H. P. and H. A. Makse. 2005. "Jamming Transition in Emulsions and Granular Materials." *Physical Review E* 72(1):11301.

Zhang, Lufeng, Fujian Zhou, Shicheng Zhang, Yuechun Wang, Jie Wang, and Jin Wang. 2019. "Investigation of Water-Sensitivity Damage for Tight Low-Permeability Sandstone Reservoirs." *ACS Omega* 4(6):11197–204.

Zhao, B., Q. Liu, and J. C. Santamarina. 2019. "Particle Migration and Clogging in Radial Flow: A Microfluidics Study." in *Trends in Mathematics*.

Zhao, Lin, Hanqiao Jiang, Jie Li, and Junjian Li. 2020. "Pore-Scale Evaluation on the Mechanism of Water Sensitivity for Sandstones Containing Non-Swelling Clays." *Arabian Journal of Geosciences* 13(2):54.

Zhou, Kang, Jian Hou, Qicheng Sun, Lanlei Guo, Shaoxian Bing, Qingjun Du, and Chuanjin Yao. 2018. "A Study on Particle Suspension Flow and Permeability Impairment in Porous Media Using LBM–DEM–IMB Simulation Method." *Transport in Porous Media* 124(3):681–98.

Zhou, Z., S. Kuang, K. Chu, and A. Yu. 2010. "Discrete Particle Simulation of Particle–Fluid Flow: Model Formulations and Their Applicability." *Journal of Fluid Mechanics* 661:482–510.